4,4'-Bis(arylideneamino)diphenyl ether Derivatives and Their Reduced Benzyl Forms: A Study on Crystal Packing Patterns and *in vitro* Cytotoxicity

Abstract

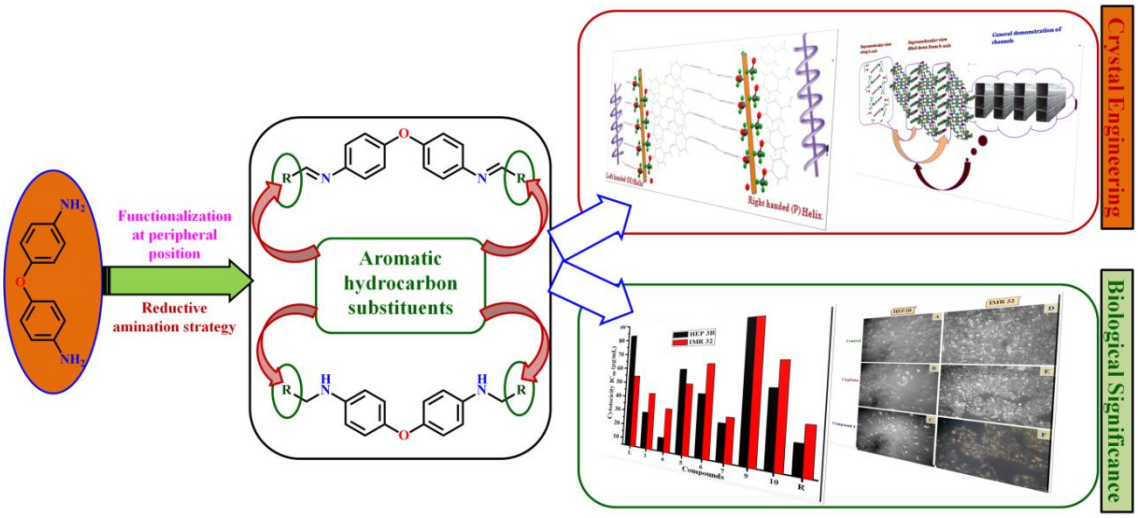

To study the impact of different polyaromatic hydrocarbon substituents and bisimine/ diamine functionalities on crystal packing and cytotoxicity, a novel series of 4,4'-bis(arylmethylideneamino)diphenyl ethers **1-6** and 4,4'-bis(arylmethylamino)diphenyl ethers **7-10** were synthesized and characterized by microanalysis, standard spectroscopic methods. The single crystal X-ray study illustrated the great impact of *para*-substituents at the peripheral phenyl rings on noncovalent interactions and hence crystal packing patterns. The crystal packing of **2** leads to attractive 2D sheets with vertically aligned helices bearing internal *racemate* in the *ab* plane through the unprecedented involvement of -OCH_3 group to favour helical contacts. The modification at the *para*-substituents efficiently switches over the dimensionality of the crystal packing in solid state. The *in vitro* cytotoxic activity profile of leader compound 4,4'-diaminodiphenyl ethers and its derivatives against two malignant human cell lines such as HEP 3B and IMR 32 determined by the MTT assay, projects compound **4** and **7** forward as more potent agents than cisplatin. The DNA fragmentation and microscopic photographs support the induction of apoptosis and explain the mode of action of these derivatives as antitumor agents.

5A.1. Introduction

Generally, the physicochemical properties of materials are often governed by the way their constituents are arranged in the solid state. Modification in molecular framework by substituent variation greatly alters the conformation and potential sites for the noncovalent interactions, which are indeed well explored in crystal engineering and medicinal chemistry. For instance, it efficiently switches over the dimensionality of the supramolecular architectures and it can provide better interactions with biomolecules which ultimately lead to the enhanced medicinal activity minimizing the undesired side effects. Pharmaceutical development for lower cost of production of generic and proprietary products using large-scale syntheses brings a new challenge in the present era. However, the lengthy synthetic protocols and complicated structure activity relationship study due to multi-functional pharmacophores is the main barrier in drug development. Hence, it becomes essential to develop simpler phamacophores with efficient synthetic procedures and screen them for desirable biological activity with high potency. Continued interest in search of novel potent anticancer compounds is mainly due to chemotherapy used in the cancer treatment always shows some undesirable side effects. Therefore, identification of new molecules that induce apoptosis i.e. nuclear condensation and DNA fragmentation by different biological as well as cytological processes is essential for the discovery and development of novel anticancer agents.[1]

Over a time period, plenty of efforts have been made in the synthesis and isolation of novel imines (>C=N-) since the first report in 1864 by Hugo Schiff. This is mainly because of their potential utilities in various fields such as synthetic, structural, medicinal and material chemistry.[2] The presence of imine (-C=N-) functionality in conjugation with polyaromatic substituents, increases the extended π-electron delocalization in the organic framework and thus significantly alters their electronic and optical properties. Imines as synthetic precursors are widely used in the development of secondary amines, which are highly versatile building blocks for various organic substrates and are essential pharmacophores in numerous biologically active compounds.[3] In the recent past, various new methods for the syntheses of secondary amines have been developed[4] but, most of these methods suffer from disadvantages such as low functional group tolerance, harsh reaction conditions, lengthy sequences and over alkylation.[5]

This chapter outlines a facile synthesis, spectral, optical and thermal characterization of 4,4'-bis(benzylideneamino)diphenyl ether, its functionalized analogues and their reduced benzyl forms (Scheme 1). The single crystal X-ray diffraction technique has been used to facilitate the understanding of structures and to review the influence of *para*-substituents of peripheral phenyl rings on the crystal packing patterns of these molecules in the solid state. A correlation between observed properties with conformational changes essentially caused by the *para*-substituents and stabilized by a diverse number of weak intermolecular interactions, have been established. Apart from this, a series of bisimine and diamine derivatives of 4,4'-diaminodiphenyl ether bearing polyaromatic hydrocarbon substituent were screened for their potential *in vitro* anticancer activity against human HEP 3B (Hepatoma) and IMR 32 (Neuroblastoma) cell lines. The impact of change in the size of polyaromatic hydrocarbon *N*-substituents in molecular framework of bisimines and diamine derivatives of 4,4'-diaminodiphenyl ether on cytotoxic activity has been investigated.

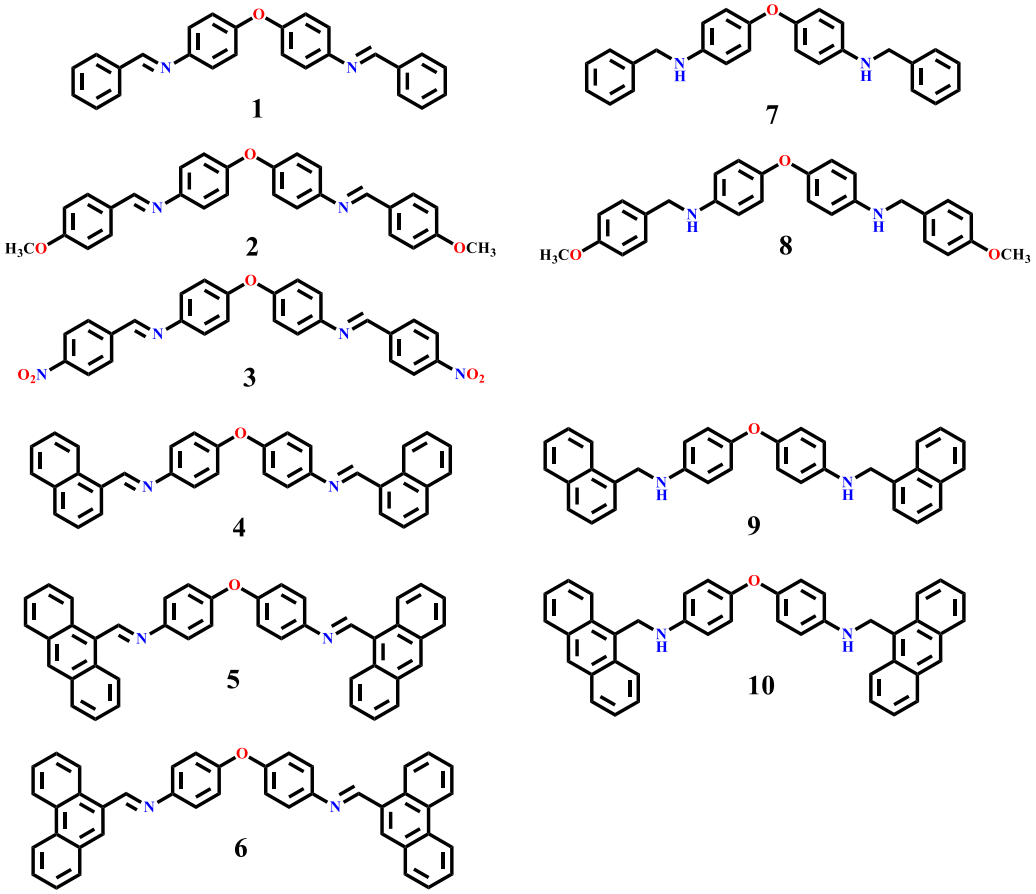

Chart 1: A series of bisimines (**1-6**) and diamines (**7-10**) under consideration.

5A.2.Experimental Section

5A.2.1 General procedure for synthesis of bisimines 1-6

In a typical synthetic procedure, 3 mmol of corresponding aldehydes (318 mg of benzaldehyde **1**, 408 mg of *p*-methoxybenzaldehyde **2**, 453 mg of *p*-nitrobenzaldehyde **3**, 469 mg of 1-naphthaldehyde **4**, 619 mg 9-formyl anthracene **5** or 619 mg 9-formyl phenanthrene **6**), a catalytic amount of glacial acetic acid and 1 mmol of 4,4'-diaminodiphenyl ether (200 mg) was added to a freshly distilled toluene (10 ml) and the reaction mixture was refluxed for 2 h using Dean-Stark apparatus. The reaction mixture was cooled at room temperature and solvent was evaporated under vacuum. The solid residue was washed with chilled absolute ethanol followed by diethyl ether and dried under vacuum to recover the product.

5A.2.2 General procedure for synthesis of diamines 7 and 10

Under nitrogen atmosphere, 2 mmol of corresponding bisimines (2 mmol, 753 mg of **1** or 2 mmol, 673 mg of **2,** 953 mg of **4** and 1153 mg of **5**) were added in 20 mL absolute ethanol and the solution was refluxed for 15 min. Excess of $NaBH_4$ (12 mmol) added to this in three portions each of 4 mmol after 30 min. The reaction mixture was allowed to reflux further for 13 hours and then it was cool at room temperature. The reaction was quenched by the addition of 5 mL conc. HCl. The reaction mixture was dried under vacuum and the residue was dissolved in 50 mL of aq. HCl (3:7; HCl: H_2O *i.e.* 3 portion HCl and 7 portion H_2O v/v). The aqueous layer was washed 2×50 mL of dichloromethane followed by basification using the aqueous NaOH solution to pH = 8-10. The compound was extracted with dichloromethane and an organic layer was dried over anhydrous Na_2SO_4; solvent was evaporated under vacuum to recover products. Compounds were purified by column chromatography using neutral alumina and 3:1 ethyl acetate and n-hexane solvent mixture as eluent. Compounds are taken for analysis, subsequent micro-, mass- and IR analysis data and NMR data for compounds are summarized following table 1 and 2.

Table 1. Micro-, mass- and IR analysis data for compounds **1-10**.

Entry	Molecular Formula (MW)	Yield (%)	Mp (°C)	Elemental Analysis (%) Found (calculated)			ES-MS (m/z)	IR data (KBr disk) υ_{max} /cm^{-1}
				C	H	N		
1	$C_{26}H_{20}N_2O$ (376.45)	99	213	82.80 (82.95)	5.38 (5.35)	7.49 (7.44)	377.1833 (M+H), (100%); 399.1712 (M+Na), (30%)	3059, 2874, 1617, 1580, 1491, 1444, 1357, 1276, 1097, 842, 749, 685, 537, 408.
2	$C_{28}H_{24}N_2O_3$ (436.50)	95	239	77.08 (77.04)	5.52 (5.54)	6.45 (6.42)	437.2131 (M+H); (10%)	2952, 2835, 1620,1605, 1508, 1497, 1413, 1360, 1306, 1281, 1245, 1166, 1103, 1024, 845, 806, 752, 721, 598, 545.
3	$C_{26}H_{18}N_4O_5$ (466.44)	95	186	66.95 (66.89)	3.89 (3.86)	12.05 (12.01)	467.1381 (M+H), (7%), 489.1036 (M+Na); (5%)	3098, 2835, 1684, 1653, 1594, 1580, 1522, 1494, 1340, 1242, 1186, 1102, 1006, 853, 833 744, 685, 590, 526, 417.
4	$C_{34}H_{24}N_2O$ (476.57)	>98	133.3	85.76 (85.69)	5.20 (5.08)	5.92 (5.88)	476.24 (4%)	3042, 2830, 1608, 1483, 1334, 1276, 1239, 1194, 1161, 1099, 831, 794, 769.
5	$C_{42}H_{28}N_2O$ (576.68)	97	197.0	87.55 (87.47)	4.98 (4.89)	4.95 (4.86)	576.49 (40%), 577.48 (34%), 578.53 (24%)	3042, 2874, 1664, 1617, 1555, 1530, 1488, 1443, 1312, 1242, 1144, 954, 881, 724.
6	$C_{42}H_{28}N_2O$ (576.68)	91	…	87.55 (87.47)	4.50 (4.89)	4.94 (4.86)	577.50 (2%)	3042, 2906, 1664, 1617, 1555, 1530, 1488, 1443, 1312, 1242, 1144, 994, 881, 724.
7	$C_{26}H_{24}N_2O$ (380.48)	78	101	82.07 (82.07)	6.35 (6.36)	7.41 (7.36)	380.2657 (M+H); (10%)	3390, 3370, 3053, 2829, 1606, 1590, 1511, 1449, 1399, 1303, 1250, 1113, 820, 741, 694, 517, 441, 416.
8	$C_{28}H_{28}N_2O_3$ (440.53)	75	165	76.31 (76.34)	6.38 (6.41)	6.41 (6.36)	439.2064 (M+H), (10%); 463.1949 (M+Na), (20%)	3384, 3355, 3048, 2824, 1620, 1602, 1510, 1497, 1312, 1278, 1220, 1119, 1083, 1027, 1004, 822, 730, 688, 509, 433.
9	$C_{34}H_{28}N_2O$ (480.60)	70	…	85.12 (84.97)	5.98 (5.87)	5.99 (5.83)	480.18(5%)	3373, 3012, 1597, 1513, 1497, 1390, 1309, 1222, 1110, 1063, 864, 825, 802, 772.
10	$C_{42}H_{32}N_2O$ (580.72)	55	…	86.98 (86.87)	5.69 (5.55)	4.99 (4.82)	581.71 (2%)	3389, 2958, 1617, 1510, 1494, 1396, 1306, 1261, 1216, 1105, 1094, 1012, 867, 814, 794, 730.

Table 2. NMR spectral data for **1-10**.

Entry	Structures	NMR Data (ppm)				
		^{1}H and ^{13}C			2D NMR Correlation expts.	
		^{1}H NMR	^{13}C NMR	DEPT-135	^{1}H-^{1}H (COSY)	^{1}H-^{13}C (HSQC)
1	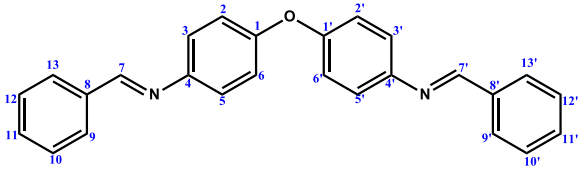	7.10 (d, 4H, **3,5,3',5'**), 7.27 (dd, 4H, **2,6,2',6'**), 7.5 (dd, 6H, **9,13,9',13'**), 7.93 (q, 4H, **10,11, 12,10',11',12'**), 8.51 (s, 2H, **7,7'**).	119.44 **(3,5,3',5')**, 122.35 **(2,6,2',6')**, 128.77, 131.32, 136.26 **(9-13,9'-13')**, 147.35 **(8,8')**, 155.76 **(1,1')**, 159.56 **(7,7')**.	--	--	--
2	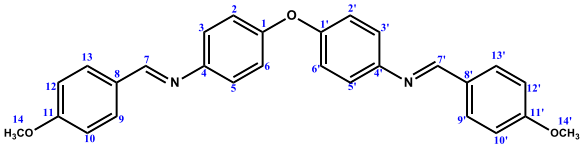	3.901 (s, 6H, **14,14'**), 7.01 (d, 4H, **3,5,3',5'**), 7.07 (d, 4H, **2,6,2',6'**), 7.25 (d, 4H, **9,13,9',13'**), 7.80(d, 4H, **10, 12,10',12'**), 8.44 (s, 2H, **7,7'**).	55.42 **(14,14')**, 114.20, 117.97 **(3,5,3',5')**, 122.21**(2,6,2',6')**, 129.33, 130.33, 130.41 **(9,10,12,13,9',10',12',13)**, 147.64 **(8,8')**, 155.50 **(1,1')**, 158.90 **(7,7')**.	55.44 **(14,14')**, 114.20, 117.95 **(3,5,3',5')**, 122.22 **(2,6,2',6')**, 129.33, 130.33, 130.42 **(9,10,12,13,9',10',12',13)**, 158.90 **(7,7')**.	--	--
3	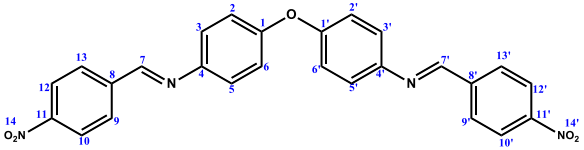	7.1(d, 4H, **3,5,3',5'**), 7.33(d, 4H, **2,6,2',6'**), 8.1(d, 4H, **9,13,9',13'**), 8.34(d, 4H, **10, 12,10',12'**), 8.605(s, 2H, **7,7'**).	119.60 **(3,5,3',5')**, 122.70 **(2,6,2',6')**, 124.04, 129.30 **(9,10,12,13,9',10',12',13')**, 141.62, 146.24 **(8,8')**, 149.24 **(11,11')**, 156.43 **(1,1')**, 156.31 **(7,7')**.	119.61 **(3,5,3',5')**, 122.71 **(2,6,2',6')**, 124.06, 129.31 **(9,10,12,13,9', 10',12',13')**, 156.35 **(7,7')**.	7.1 **(3,5,3',5')** couple with 7.3 **(2,6,2',6')**, 8.1 **(9,13,9',13')** couple with 8.3 **(10, 12,10',12')**, 8.605 **(7,7')**.	--

4	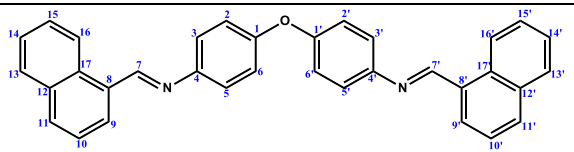	7.185 (d, 4*H*, **3,5,3',5';** J=8.4 Hz); 7.390 (d, 4*H*, **2,6,2',6';** J=8.4 Hz); 7.619 (m, 4*H*, **11,15,11',15';** J=8.4, 8.0, 7.2 Hz); 7.680 (dd, 2*H*, **10,10'**; J=8.0, 7.2 Hz); 7.964 (d, 2*H*, **13,13';** J=8.0 Hz); 8.013 (d, 2*H*, **14,14';** J=8.0 Hz); 8.146 (d, 2*H*, **16,16';** J=7.2 Hz); 9.110 (d, 2*H*, **9,9'**; J=8.4 Hz); 9.177 (s, 2*H*, **7,7'**).	119.60 **(3,5,3',5')**, 122.52 **(2,6,2',6')**, 124.33 **(9,9')**, 125.42, 126.32 **(11,15,11',15')**, 127.55 **(10,10')**, 128.88 **(13,13')**, 129.87 **(16,16')**, 131.53 **(12,17, 12',17')**, 131.96 **(14,14')**, 133.98 **(8,8')**, 148.02 **(4,4')**, 155.87 **(1,1')**, 159.34 **(7,7')**.	119.57 **(3,5,3',5')**, 122.48 **(2,6,2',6')**, 124.26 **(9,9')**, 125.39, 126.30 **(11,15, 11',15')**, 127.52 **(10,10')**, 128.85 **(13,13')**, 129.80 **(16,16')**, 131.95 **(14,14')**, 159.34 **(7,7')**.	7.185 (**3,5,3',5'**) couple with 7.390 (**2,6,2',6'**); 7.619 (**11, 15, 11',15'**) couple with 7.680 (**10, 10'**), 7.964 (**13,13'**), 8.013 (**14,14'**) and 8.146 (**16,16'**); 7.680 (**10, 10'**) couple with 9.110 (**9,9'**).	7.185 (**3,5,3',5'**) and 119.57 (**3,5,3',5'**); 7.390 (**2,6,2',6'**) and 122.48 (**2,2',6,6'**); 7.619 (**11,15,11',15'**) and 125.39, 126.30 (**11,15,11',15'**), 7.680 (**10,10'**) and 127.52 (**10,10'**); 7.964 (**13,13'**) and 128.85 (**13,13'**); 8.013 (**14,14'**) and 131.95 (**14,14'**); 8.146 (**16,16'**) and 129.80 (**16,16'**); 9.110(**9,9'**) and 124.26 (**9,9'**); 9.177 (**7,7'**) and 159.34 (**7,7'**).
5	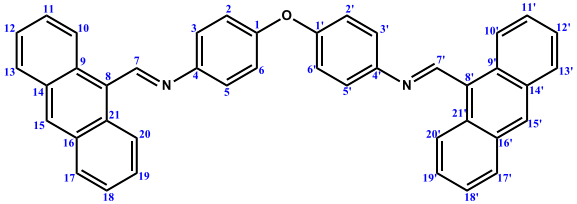	6.650 (d, 4*H*, **3,5,3',5';** J=6.8 Hz)[a]; 6.740 (d, 4*H*, **3,5,3',5';** J=6.8 Hz)[b]; 6.840 (d, 4*H*, **2,6,2',6';** J=6.8 Hz)[a]; 6.980 (d, 4*H*, **2,6,2',6';** J=6.8 Hz)[b]; 7.107 (d, 2*H*, **13,13';** J=8.8 Hz)[b]; 7.272 (d, 2*H*, **13,13';** J=7.6 Hz)[a]; 7.440 (d, 2*H*, **12,12'** J=6.8 Hz)[b]; 7.510-7.616 (m, **11,17,18,19, 11',17',18',19'**)[a+b];	116.25 (**3,5,3',5'**)[a]; 116.34 (**3,5,3',5'**)[b]; 118.07 (**13,13'**)[b]; 119.55 (**2,6,2',6'**)[a]; 119.69 (**13,13'**)[a]; 121.04 (**2,6,2',6'**)[b]; 122.38 (**12,12'**)[b]; 122.61 (**12,12'**)[a]; 124.77 (**20,20'**)[a]; 124.82(**20,20'**)[b]; 125.43, 125.47, 127.22, 127.33 **(11,17,18,19,11',17' ,18',19')**[a+b]; 127.53 **(14,14')**[a]; 129.06 **(10,10')**[b]; 129.11 **(10,10')**[a]; 130.50	116.24 (**3,5,3',5'**)[a]; 116.33 (**3,5,3',5'**)[b]; 118.06(**13,13'**)[b]; 119.54 (**2,6,2',6'**)[a] 119.68 (**13,13'**)[a]; 121.04 (**2,6,2',6'**)[b]; 122.37(**12,12'**)[b]; 122.60(**12,12'**)[a]; 124.77(**20,20'**)[a]; 124.81(**20,20'**)[b]; 125.42,125.47, 127.22,127.33	6.650 (**3,5,3',5'**)[a] couple with 6.840 (**2,6,2',6'**)[a]; 6.740 (**3,5,3',5'**)[b] couple with 6.980 (**2,6,2',6'**)[b]; 7.107(**13,13'**)[b] couple with 7.440 (**12,12'**)[b]; 7.510-7.616 (**11,17,18,19, 11',17',18',19'**)[a+b] couple with 7.272 (**13,13'**)[a], 8.060(**10,10'**)[b], 8.079 (**10,10'**)[a], 8.737 (**20,20'**)[b]	6.650(**3,5,3',5'**)[a] and 116.25 (**3,5,3',5'**)[a]; 6.740 (**3,5,3',5'**)[b] and 116.34 (**3,5,3',5'**)[b]; 6.840 (**2,6,2',6'**)[a] and 119.55 (**2,6,2',6'**)[a]; 6.980 (**2,6,2',6'**)[b] and 121.04 (**2,6,2',6'**)[b]; 7.107(**13,13'**)[b] and 118.07 (**13,13'**)[b]; 7.272 (**13,13'**)[a] and 119.69 (**13,13'**)[a]; 7.440 (**12,12'**)[b] and 122.38 (**12,12'**)[b]; 7.510-7.616 (**11,17,18,19, 11',17',18',19'**)[a+b] and 125.43, 125.47, 127.22, 127.33 (**11,17,18,19,**

		8.060 (d, 2*H*, **10,10';** J=7.2 Hz)[b]; 8.079 (d, 2*H*, **10,10';** J=7.2 Hz)[a]**;** 8.557 (s, 2*H*, **15, 15'**)[b]; 8.580 (s, 2*H*, **15, 15'**)[a]; 8.737 (d, 2*H*, **20, 20';** J=8.8 Hz)[b]; 8.782 (d, 2*H*, **20, 20';** J=8.8 Hz)[a]**;** 9.695 (s, 2*H*, **7,7'**)[b]; 9.745 (s, 2*H*, **7,7'**)[a].	**(15, 15')**[b]; 130.59, 130.65 **(14,16,14',16')**[b]**;** 130.72 **(15,15')**[a]; 131.35 **(16,16')**[a], 141.70 **(9, 21, 9', 21')**[a]; 142.81 **(9, 21, 9', 21')**[b]; 146.88 **(8,8')**[b]; 148.02 **(8,8')**[a]; 148.80 **(4,4')**[b]; 150.62**(4,4')**[a]; 156.11 **(1,1')**[a]; 157.75 **(1,1')**[b], 158.48 **(7,7')**[b]; 159.09 **(7,7')**[a].	**(11,17,18,19,11',17',18',19')**[a+b]; 129.06**(10,10')**[b]; 129.11**(10,10')**[a]; 130.49 **(15, 15')**[b]; 130.72 **(15,15')**[a]; 158.48 **(7,7')**[b]; 159.09 **(7,7')**[a].	and 8.782 **(20,20')**[a].	**11',17',18',19')**[a+b]**;** 8.060**(10,10')**[b] and 129.06 **(10,10')**[b]; 8.079 **(10,10')**[a] and 129.11 **(10,10')**[a]; 8.557 **(15,15')**[b] and 130.49 **(15,15')**[b]; 8.580 **(15,15')**[a] and 130.72 **(15,15')**[a]; 8.737**(20,20')**[b] and 124.82 **(20,20')**[b]; 8.782 **(20,20')**[a] and 124.77**(20,20')**[a]; 9.695 **(7,7')**[b] and 158.48 **(7,7')**[b]; 7.974 **(7,7')**[a] and 159.09 **(7,7')**[a].
6	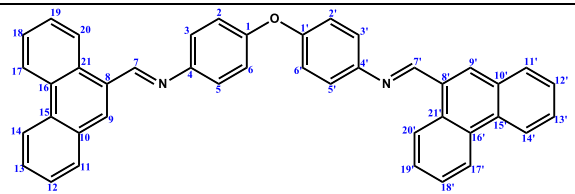	7.260 (d, 4*H*, **3,5,3',5';** J=5.6 Hz); 7.51 (d, 4H, **2,6,2',6';** J=5.6 Hz); 7.574 (m, 4*H*, Ph); 7.835 (m, 2*H*, Ph) 8.085 (d, 4*H*, **11,11',20',20'**; J=4.8 Hz); 8.345 (d, 4*H*, Ph; J=5.6Hz); 8.604 (s, 2*H*, **9,9'**); 8.785 (d, 2*H*, Ph; J=8.8 Hz); 9.753 (s, 2*H*, **7,7'**).	119.68, 121.94, 122.61, 122.66, 123.56, 124.75, 125.46, 125.73, 126.58, 126.93, 127.24, 127.33, 127.64, 128.58, 129.10, 129.19, 129.33, 129.62, 130.28, 130.64, 130.73, 131.09, 131.34, 132.03, 132.66, 133.49, 134.15, 135.35, 137.15, 144.78, 147.90 (Ph), 156.13(**1,1'**),	--	--	--

			159.16(**7,7'**).			
7	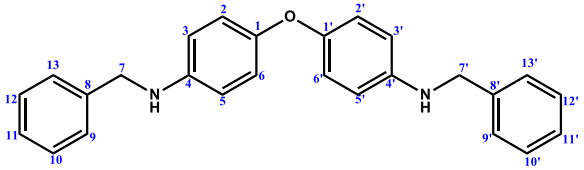	3.828 (broad, 2*H*, ***NH***), 4.305 (s, 4*H*, **7,7'**); 6.6 (dd, 4*H*, **3,5,3',5**), 6.84 (dd, 4*H*, **2,6,2',6'**), 7.303 (m, 10*H*, **9-13,9'-13'**).	49.04 **(7,7')**, 113.81, 119.54, 127.22, 127.55, 128.61, 139.49, 143.90, 150.03 (all corresponds to the carbons of Ph).	49.02 **(7,7')**, 113.79, 119.54, 127.24, 127.56, 128.62 (all CH of Ph).	--	--
8	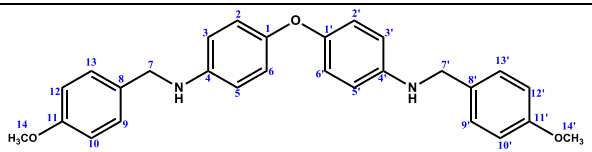	3.586 (broad, 2*H*, ***NH***), 3.828, 3.894 (s, 3H, **14,14'**), 4.235 (s, 4*H*, **7,7'**), 6.6 (dd, 4*H*, **3,5,3',5**), 6.860 (dd, 8*H*, -Ph), 7.729 (m, 4*H*, -Ph).	49.19 **(14,14')**, 55.28**(7,7')**, 114.02, 114.22, 114.94, 119.54, 129.19, 130.52, 159.02 (all corresponds to the carbons of Ph)	--	--	--
9	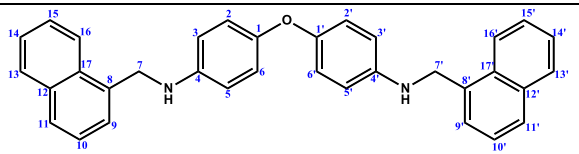	3.750 (broad s, 2*H*, ***NH***); 4.733 (s,4*H*,**7,7'**); 6.676(d,4*H*,**3,5,3',5;** J=8.8 Hz); 6.924(d,4*H*, **2,6,2',6';** J=8.8 Hz); 7.476(m,2*H*, **10,10'**) (J=7.2 Hz); 7.565(m,6*H*,**11,14,15,11',14',15'**; J=7.2, 2.4 Hz); 7.855(d,2*H*, **9,9'**) (J=7.64 Hz); 7.935(d,2*H*, **13,13';** J=8.8 Hz); 8.120(d,2*H*,**16,16'**; J=7.2 Hz).	47.12**(7,7')**, 113.74 **(3,5,3',5')**, 119.66 **(2,6,2',6')**, 123.68**(16,16')**, 125.61**(10,10'),** 125.90, 126.14 and 126.39 **(11,14,15,11'14',15')**, 128.23(**9,9'),** 128.82 **(13,13')**, 131.58 **(12,12')**, 133.89 **(17,17')**, 134.46 **(8,8'),** 144.07 **(4,4'),** 150.05 **(1,1'),**	47.10 and 47.12 **(7,7')**, 113.74 and 113.75 **(3,5,3',5')**, 119.70 **(2,6,2',6')**, 123.71**(16,16')**, 125.64 **(10,10')**, 125.94, 126.15 and 126.42 **(11,14,15,11'14',15')**, 128.25(**9,9'),** 128.85**(13,13')**.	6.67 (**3,5,3',5'**) couple with 6.924 (**2,6,2',6'**); 7.476 (**10,10'**) couple with 7.855 (**9,9'**) and 7.566 **(11,14,15,11'14',15')**; 7.566 **(11,14,15,11'14',15')** couple with 7.576 **(10,10')**, 7.935 **(13,13')** and 8.120 **(16,16')**.	4.733(**7,7'**) and 47.10, 47.12**(7,7')**; 6.676(**3,5,3',5'**) and 113.74, 113.75; 6.924(**2,6,2',6'**) and, 119.70**(2,6,2',6')**; 7.476 (**10,10'**) and 125.64(**10,10'**); 7.566 **(11,14,15,11'14',15')** and 125.94, 126.15, 126.42**(11,14,15,11'14',15');** 7.855 (**9,9'**) and 128.25 (**9,9'**); 7.935 **(13,13')** and 128.85**(13,13')**; 8.120 **(16,16')** and 123.71 **(16,16')**.

10	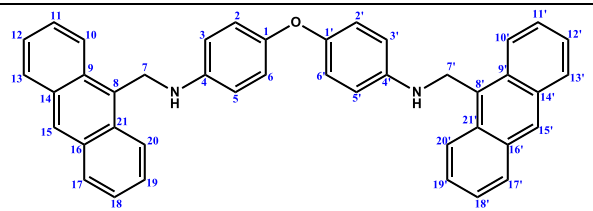	3.688(bs, 2*H*, **NH**); 5.153(s, 2*H*, **7,7'**)[a], 5.177 (s, 2*H*, **7,7'**)[b]; 6.653 (d, 4*H*, **3,5,3',5'**)[b], 6.670 (d, 2*H*, **3,3';** J=8.8 Hz)[a], 6.800 (d, 2*H*, **5, ,5'**)[a]; 6.820 (d, 4*H*, **2,6,2',6'** J=8.8 Hz)[b]; 6.890 (d, 2*H*, **2,2'**; J=8.8 Hz)[a]; 6.985 (d, 2*H*, **6,6'**; J=8.8 Hz)[a]; 7.030 (d,2*H*, **13,13';** J=8.8 Hz)[b]; 7.050 (d,2*H*, **13,13';** J=8.8 Hz)[a]; 7.515 (m,10*H*, **11,12,17,18,19, 11',12',17',18',19';** J=8.8, 1.9 Hz)[a+b]; 8.060 (d, 2*H*, **10, 10';** J=8.8 Hz)[b]; 8.078 (d, 2*H*, **10, 10';** J=8.8 Hz)[a]; 8.315 (d, 2*H*, **20, 20';** J=8.8 Hz)[a]; 8.335 (d, 2*H*, **20, 20';** J=8.8 Hz)[b]; 8.510(s, 2*H*, **15,15'**)[a+b].	41.53 **(7,7')**[a+b], 113.58 **(5,5')**[a], 113.68 **(2,6,2',6')**[b], 116.24 **(3,5,3',5')**[b], 116.29 **(3,3')**[a], 119.46 **(2,6,2',6')**[a], 119.55 **(2,6,2',6')**[b], 119.76 **(13,13')**[b], 119.85 **(13,13')**[a], 124.21**(20,20')**[a+b], 125.19 and 126.50 (**11,12,17, 18,19, 11', 12',17', 18',19')**[a+b], 127.95 **(15,15')**[a+b], 129.15 **(10,10')**[a+b], 130.45 **(9,21,9',21')**[a], 131.52 **(9,21,9',21')**[b], 141.63 **(14,16,14',16')**[a], 141.69 **(14,16,14',16')**[b], 144.40 **(4,4')**[a+b], 149.93, 150.20**(1,1')**[b], 150.61, 150.88**(1,1')**[a].	41.493 **(7,7')**[a+b], 113.58 **(5,5')**[a], 113.62 **(2,6,2',6')**[b], 116.24 **(3,5,3',5')**[b], 116.29 **(3,3')**[a], 119.46 **(2,6,2',6')**[b], 119.55 **(2,6,2',6')**[b], 119.76 **(13,13')**[b], 119.85 **(13,13')**[a], 124.21 **(20,20')**[a+b], 125.19 and 126.50 (**11,12,17, 18,19, 11', 12',17', 18',19')**[a+b], 127.95 **(15,15')**[a+b], 129.15**(10,10')**[a+b].	6.653 **(3,5,3',5')**[b] couple with 6.820 **(2,6,2',6')**[b] ; 6.670 **(3,3')**[a] couple with 6.890 **(2,2')**[a]; 6.800 (**5, ,5')**[a] couple with 6.985 **(6,6')**[a]; 7.515(**11,12,17,18, 19, 11',12',17', 18', 19')**[a+b] couple with 7.030 **(13,13')**[b], 7.050 **(13,13')**[a], 8.060 **(10, 10')**[b]; 8.078 **(10, 10')**[a]; 8.315 **(20, 20')**[a] and 8.335 (**20, 20')**[b].	5.153 **(7,7')**[a], 5.177 **(7,7')**[b] and 41.493**(7,7')**[a+b]; 6.653 **(3,5,3',5')**[b] and 116.24 **(3,5,3',5')**[b]; 6.670 **(3,3')**[a] and 116.29 **(3,3')**[a]; 6.800 (**5, ,5')**[a] and 113.58 **(5,5')**[a]; 6.820 **(2,6,2',6')**[b] and 113.62, 119.55 **(2,6,2',6')**[b]; 6.890 **(2,2')**[a], 6.985 **(6,6')**[a] and 119.46 **(2,6,2',6')**[b]; 7.030 **(13,13')**[b] and 119.76 **(13,13')**[b]; 7.050 **(13,13')**[a] and 119.85 **(13,13')**[a]; 7.515 **(11,12,17,18,19, 11',12',17', 18', 19')**[a+b] and 125.19 and 126.50 **(11,12,17, 18,19, 11', 12',17', 18',19')**[a+b]; 8.060 **(10, 10')**[b], 8.078 **(10, 10')**[a] and 129.15 **(10,10')**[a+b]; 8.315 **(20, 20')**[a], 8.335 (**20, 20')**[b] and 124.21 **(20,20')**[a+b]; 8.510(s, 2*H*, **15,15'**)[a+b] and 127.95 **(15,15')**[a+b].

5A.3.Results and discussion

5A.3.1 Synthesis and characterization

Bisimine derivatives 4,4'-bis(arylmethylideneamino)diphenyl ethers **1-6** were obtained in >80% yield by condensation of 4,4'-diaminodiphenyl ether with different aromatic aldehydes (Scheme 1). Practically, the reaction mixtures were refluxed in toluene containing a catalytic amount of glacial acetic acid by using a Dean-Stark apparatus. Dean-Stark apparatus was helpful in removing H_2O molecules formed during the course of the reaction as azeotropic mixture and thereby shifts the equilibrium towards a product, with higher yield and in less time. This synthetic method was found to be superior over a number of reported methods which are time consuming and produce relatively low yields. Diamines derivatives 4,4'-bis(arylmethylamino)diphenyl ethers **7-10** were synthesized by reduction of corresponding bisimines with $NaBH_4$ in ethanol in good yield. One remarkable observation was made during the reduction is that all the bisimines were readily reduced except **3**; probably due to the extra stability of –C=N bond conferred by *p*-NO_2 groups. The reductive amination strategy used for the reduction of these compounds is found to be superior over several conventional procedures.[5] The elemental analysis data for **1-10** are in good agreement with their compositions.

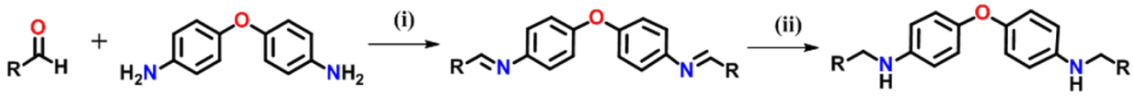

(i) = Toluene; reflux
(ii) = $NaBH_4$; EtOH abs

Scheme 1. Synthetic protocol for 4,4'-diaminodiphenyl ether derivatives.

A series of compounds synthesized were characterized by elemental analysis, and by relevant spectroscopic techniques, mass, IR, UV-visible, NMR (^{1}H, ^{13}C, DEPT-135) and 2D NMR (gCOSY, HSQC) spectroscopy. The unambiguous structure of **1-3** and **7** were elucidated by single crystal X-ray diffraction study. The elemental analysis data for **1-10** are in good agreement with their compositions. The IR, NMR and UV-visible spectra of these compounds are consistent with their chemical formula determined by elemental analysis and further confirmed by mass spectral analysis. Characterization data is summarized in Table 1 and 2.

In IR spectrum of bisimines **1-6**, the most characteristic band appeared in the region of 1684-1580 cm^{-1}, is due to ν(C=N) whereas diamines **7-10** displayed ν(N-H) bands in the region of 3390-3355 cm^{-1}, respectively. All the compounds showed a weak

intensity bands in the regions of 3012-2830 cm^{-1} due to the aromatic, benzylidene and benzyl ν(C-H) stretching vibrations respectively. The appearance of a very strong band in the region of 881-814 cm^{-1} due to the aromatic ν(C-H) out-of plane bending vibrations suggests the presence of *para*-disubstituted benzene rings. Apart from these bands, medium intensity bands appeared in the region of 1664-1443 cm^{-1} and 1360-994 cm^{-1} are due to aromatic ring ν(C=C) and ν(C-O) /ν(C-N) stretching vibrations, respectively.

The ^{1}H NMR spectrum of bisimines **1-6** showed most characteristic signals in the region of δ = 8.44-9.76 ppm due to imine functionality along with the corresponding signals due to aromatic protons. It appeared that this ^{1}H signal is significantly upfield shifted in compound **2** and downfield shifted in compound **3** as compared to its position in compound **1**, due to the reverse effect of *p*-OCH_3 and *p*-NO_2 substituents of **2** and **3**, respectively. A significant downfield shifting of HC=N signals are observed as the number of aromatic rings are increased on -HC=N functionality. The diamines **7-10** showed most characteristic signals as broad singlet in the range of δ = 3.828-3.586 ppm due to -NH functionality and a sharp singlet in the range of δ = 4.235-5.18 due to -CH_2Ar benzylic protons, respectively. In addition, compound **2** and **8** shows signals at δ = 3.901 and 3.807 ppm due to –OCH_3. Other signals are observed due to aromatic protons with proper splitting patterns and the assignment each ^{1}H signals are well supported by ^{13}C and DEPT-135 NMR experiments for relevant compounds. In the ^{13}C and DEPT-135 NMR spectra of bisimines **1-6**, the characteristic signals appeared in the range of δ = 155-160 ppm are attributable to C=N carbon atoms whereas compounds **2** and **8** show ^{13}C signals at δ = 55.42 and 55.28 ppm, respectively due to -OCH_3 functionality. For diamines **7-10**, signals appeared in the range of δ = 40-50 ppm is assigned to benzylic CH_2 carbon atoms. All other signals observed in the range of δ = 110-155 ppm are due to aromatic carbons. The IR, ^{1}H and ^{13}C NMR spectral data for **1-5** are in good agreement with those observed for the similar compounds reported in the literature. Furthermore, to reinforce the assignments of the NMR data and to obtain the detailed view of the structural elucidation, experiments were carried out using 2D NMR spectroscopy such as homonuclear gCOSY and heteronuclear HSQC experiments on some of the relevant compounds.

Interestingly, ^{1}H and ^{13}C NMR data along with 2D NMR study of bisimine **5** bearing anthracenyl substituents at the peripheral positions, suggest the presence of two

isomeric species in 43:57 ratios. The possibility of the existence of both E/Z isomers in **5** was ruled out as it maintains almost the similar ratios (42:58) even on complete reduction to its benzyl form **10**. Probably, in the presence of the bulkier anthracenyl group, the possible C-C bond rotation is hindered and hence compound **5** and **10** could exist in the form of 43:57 and 42:58 conformer mixtures (a and b), respectively.[6]

COSY experiments of **4** and **5** clearly show correlations between the peak at 7.185/7.390 ppm and 6.650/6.840[a], 6.740/6.980[b] ppm, respectively. HSQC experiment of **4** shows cross peaks at 7.185/119.60 and 7.390/122.48 whereas compound **5** shows cross peaks at 6.650/116.25[a], 6.740/116.34[b], 6.840/119.55[a], 6.980/121.04[b]. These correlations support the assignment of signals corresponding to diphenyl ether moieties in the molecular framework. Moreover, the COSY experiment of **4** and **5** does not show any correlation for the peak 9.177 and 9.745[a], 9.695[b] respectively whereas HSQC experiment of **4** and **5** shows cross peaks at 9.177/159.34 and 9.745/159.09[a], 9.695/158.48[b] respectively. These correlations support the assignment of signals corresponding to -HC=N functionality present in the respective compounds. The COSY experiment of **9** and **10** do not show any correlation for the peak 4.733 ppm and 5.153[a], 5.177[b] ppm respectively whereas HSQC experiment shows two distinct cross peaks at 4.733/47.10, 47.12 ppm for **9** and cross peaks at 5.153[a], 5.177[b]/41.493[(a+b)] ppm respectively which are assigned to the benzylic $–CH_2$ functionality. Similarly, the assignments of remaining ^1H, ^{13}C signals are based on DEPT-135, COSY and HSQC 2D NMR experiments. The IR, ^1H, ^{13}C NMR and 2D NMR correlation experiment data for **1-6** and **7-10** are in good agreement with those observed for the similar types of compounds reported in the literature.[7] All compounds synthesized were characterized by mass spectroscopy, the peaks detected corresponding to the molecular ion m/z= (M+1) and m/z = (M+Na) gives the evidence for the formation of the compounds.

5A.3.2 Thermogravimetric studies for 1-10

A thermogravimetric study of **1-10**, performed under N_2 atmosphere from room temperature to 550 °C at a heating rate of 10 °C/min, and thermal analysis data of all the compounds is given in Table 3.

Table 3. Thermogravimetric data for **1**-**10**.

Entry	Mp °C	Mass Loss% (Temperature range °C)	Residual Content	DTG (°C)	DTA (°C)
1	185.4	99.6% (300-410)	---	410	285.4 (-6.36 uV), 400.8 (-6.43 uV)
2	238.9	73% (280-490)	27% char	171.6 239.0 417.0	238.9 (-10.22 uV), 433.5 (2.03 uV), 535.9 (-16.94 uV)
3	198.1	0.5% (125-210), 17.4% (310-400), 6.6% (400-510),	Mass loss continues after 510 °C.	198.6 341.8 371.3	198.1 (-2.58 uV) 373.4 (23.72 uV)
4	133.3	71.2% (100-500)	Mass loss continues after 550 °C	454.5	122.2 (5.51 uV), 133.3 (3.13 uV), 457.8 (-2.02 uV),
5	197.0	64.9% (100-550)	Mass loss continues after 550 °C	410.7	197.0 (3.85 uV)
6	146.4	34.4% (50-275) 37.0%(275-550) 71.4% (50-550)	Mass loss continues after 550 °C	211.1, 402.0	146.4 (4.57 uV)
7	90.0	93.0% (200-410)	7% char	380.6	90.0 (1.43 uV) 184.3 (-7.97 uV)
8	183.6	85.8% (170-300), 9.6 % (310-400).	4.6% char	273.6 357.3	183.6 (0.92 uV) 277.8 (-0.49 uV)
9	--	87.3% (100-500)	12.7 char	380.5	…
10	--	87.4% (125-550)	12.6 char	300.1, 350.3, 525.0	…

The peaks on DTG and corresponding DTA curves confirm a single or multi stage mass loss for these compounds. The DTA curves exhibits first endothermic peak without any significant mass loss on DTG curves for each compound, due to the phase change that can be assigned to the melting points of the respective compounds (except compound **9** and **10**). Other peaks of DTA curves are attributed to endothermic and/or exothermic elimination of molecular fragments due to the thermal degradation, confirmed by peaks on DTG curves. Compound **1** showed ~ 99 % mass loss up to 410 °C, which can be attributed to either almost complete thermal degradation or evaporation of compound at high temperature. Interestingly, compound **3** shows only 24% mass loss, essentially taking place in two stages, which is significantly less, as compared to all other compounds. The mass loss of **3** continues even after 550 °C. The extra thermal stability of this compound may be caused by the presence of *p*–NO_2 groups peripheral phenyl rings, which offer extended conjugation and massive number of donor/ acceptor sites for intermolecular interactions in the solid state. Smaller bond lengths, bond angles and angles of '*gauche*' conformation, revealed by single crystal X-ray study of **3**; further support the thermal stability of this compound.

5A.3.3 Effect of substituents on crystal packing patterns

The existence of C–H...O hydrogen bond, which was initially suggested by Glasstone in 1937[8] and later on by Sutor in early 1960s,[9] is now well established in the structural chemistry. Several investigations, especially on C–H...O[10] and C–H...N[11] containing C-H groups as donor groups, have been carried out. The significance of these interactions along with weak C–H...π[12] and π...π[13] interactions as a directing tool in the organization of molecules has been recognized in both chemistry and biology and thus implicated successfully in the crystal engineering[14] and supramolecular assemblies.[15] Understanding of the molecular packing is important because properties of materials are often governed by the way in which their constituent molecules are arranged.[16] That knowledge is further imperative in crystal engineering and structural chemistry to deliberately engineer the arrangement of molecules in new materials. However, predetermination of molecular packing is a big challenge to the researchers, as intermolecular forces that hold the molecules in the solid state are inadequately understood and hard to predict, particularly for organic solids.[17] Thus any step taken into predictable molecular packing is a practical movement towards the ultimate goal of structural chemistry to design new solid of desired properties.

Supramolecular structures of several organic molecules and their properties are clearly shown to be sustained *via* hydrogen bonds and π...π interactions. For instance, a clear analogy between the structures and polymorphs of methoxy-substituted distyrylpyrazines has been emerging from a detailed comparison of their supramolecular structures stabilized *via* C–H...O, π...π and C–H...N interactions.[18] It is clear that favourable non-covalent interactions between organic molecules include *π...π* and C–H...*π* interactions, nevertheless, both types of interactions appeared to be a subject of the electronic nature of substituents.[19] Furthermore, it has been demonstrated in literature that helicity in the supramolecular architecture can be induced by conformational limits of macromolecules, inter-, intra-molecular hydrogen bonds or coordination to metal ions. A majority of helical molecular assemblies in the crystalline phase reported to date have been constructed by the use of achiral building blocks.[20]

X-ray crystallography and data collection: Crystals of **1-3** and **7** suitable for X-ray crystallographic study were obtained in dichloromethane by slow evaporation at 4 °C. Intensity data were collected on Oxford diffraction X Calibur diffractometer equipped with Eos CCD detector at 150 K for $[C_{26}H_{20}N_2O]$ **1** and $[C_{26}H_{18}N_4O_5]$ **3** and at 298 K

for [$C_{28}H_{24}N_2O_3$] **2** and [$C_{26}H_{24}N_2O$] **7**, respectively. Monochromatic Mo-*Kα* X-ray (λ=0.71073 Å) radiation was used for the measurements. Data were collected and reduced by using the ''CrysAlispro'' program.[21] An empirical absorption correction using spherical harmonics was implemented in ''SCALE3 ABSPACK'' scaling algorithm. The crystal structures were solved by direct methods using SHELXL-97[22] and the refinement was carried out against F^2 using SHELXL-97 program package.[23] All non-hydrogen atoms were refined anisotropically.

Structural descriptions: Block shaped colourless crystals for **1**, **2**, **7** and golden-yellow crystals for compound **3**, suitable for single crystal X-ray diffraction study, were grown from dichloromethane solution by slow evaporation at 4 °C. The crystal data and structure refinement for **1**-**3** and **7** are given in Table 4.

Table 4. Crystal data and structure refinement for compounds **1, 2, 3** and **7**.

	1	**2**	**3**	**7**
Formula	$C_{26}H_{20}N_2O$	$C_{28}H_{24}N_2O_3$	$C_{26}H_{18}N_4O_5$	$C_{26}H_{24}N_2O$
Formula weight	376.44	436.49	466.44	380.47
Cell volume (Å3)	1917.1(2)	2234.1(4)	1112.71	2077.6(3)
T (K)	148	298(2)	150	293(2)
Crystal System	Monoclinic	Orthorhombic	Triclinic	Orthorhombic
Space group	P 2_1/n	C 2 c b	P -1	Pbna
Z	4	4	2	4
Completeness to theta (%)	(θ = 24.99°) 93.7	(θ = 26.36°) 99.8	(θ = 25.00°) 99.1	(θ =26.37°) 96.6
a(Å)	6.0480(3)	6.1649(7)	8.3067(8)	6.4655(7)
b(Å)	43.160(4)	48.861(5)	9.0591(9)	42.771(4)
c(Å)	9.5052(5)	7.4168(7)	17.0515(17)	7.5129(7)
α(°)	90.00	90.00	74.718(9)	90.00
β(°)	129.407(3)	90.00	78.865(8)	90.00
γ(°)	90.00	90.00	64.522(10)	90.00
Goodness-of-fit on F^2	0.976	0.992	1.007	0.994
Calculated density (mg m^{-3})	1.304	1.298	1.392	1.216
Absorption coefficient (mm^{-1})	0.080	0.085	0.099	0.074
F(000)	792	920	484	808
θ range for data collection (°)	3.36-24.99	2.741-28.887	3.44-25.00	2.86-26.37
Index ranges	– 7<=h<=6, – 49<=k<=51, – 11<=l<=10	– 7<=h<=7, – 60<=k<=60, – 9<=l<=9	– 9<=h<=9, – 10<=k<=10, – 20<=l<=19	– 4<=h<=8, – 53<=k<=49, – 4<=l<=9
Reflections collected	12869	10072	7621	5199
Data / restraints / parameters	3159/0/ 262	2219/1/152	3887/0/316	2055/0/136
Largest diff. peak/ hole (e A^{-3})	0.219/-0.230	0.133/-0.167	0.171/-0.199	0.141/-0.210
Final R indices [I>2σ(I)]	R1 = 0.0742, wR2 = 0.1409	R1 = 0.0500, wR2 = 0.0789	R1 = 0.0422, wR2 = 0.1017	R1 = 0.0604, wR2 = 0.0919
R indices (all data)	R1 = 0.1100, wR2 = 0.1530	R1 = 0.1139, wR2 = 0.0987	R1 = 0.0666, wR2 = 0.1088	R1 = 0.1453, wR2 = 0.1219

Table 5. Significant intermolecular interactions [Interatomic distances (Å), and bond angles (°)] found in compounds **1**-**3** and **7**.

Compounds	D─H…A	D─H	H…A	D…A	<DHA
1	C_{15}─H_{15}…C_{g1}	0.950	2.767	3.522	137.03
	C_{13}─H_{13}…C_{g2}	0.950	2.786	3.549	137.91
2	C_{14}─H_{14}…O_2	0.960	2.574	3.433	149.00
3	C_{25}─H_{25}…N_2	0.951	2.615	3.408	141.12
	C_g…C_g	--	--	3.872	--
	C_7─H_7…O_1	0.950	2.516	3.319	142.32
	C_{13}─H_{13}…O_2	0.950	2.720	3.573	149.81
	C_{14}─H_{14}…O_4	0.950	2.548	3.353	142.70
7	C_{13}─H_{13}…C_g	0.930	2.717	3.574	153.71

Evidently, a change in the *para*-substituents of peripheral phenyl rings in **1**-**3** and a change of imine functionalities of **1** to amine **7**, changes the electronic nature as well as stereochemical conformations of the molecules. This can be visualized clearly from the different dihedral angles between the least squares planes through the benzene rings. The imine functionalities lead to the rigidity as well as extended conjugation in **1** and **2**, hold the phenyl rings adjacent to imine moiety virtually planar. The angle between the plane through one peripheral ring and the plane through the central ring is about 8.81° and 5.27°, while the angle between the plane through the central ring and the plane through other peripheral ring is about 5.95° and 5.27° for **1** and **2**, respectively. In contrast, these phenyl rings are in different conformational modes in compound **3** and the central phenyl rings are twisted out of the plane of the peripheral phenyl rings by 53.09° and 18.02°, respectively. It appears that *the p - NO_2 group* positioned on peripheral phenyl rings has a large enough effect on these conformational changes and molecules of **3** are indeed stabilized by a great number of weak interactions. In the case of compound **7**, reduction of the imine functionality diminishes extended conjugation causing easy accessibility of bonds for free rotations leading to flexibility in the molecule. Thus stable '*gauche*' conformational modes are attained by these phenyl rings *i.e.* central phenyl rings are twisted out of the plane of the peripheral phenyl rings by 74.03°. These changes (*vide supra*) lead to a scope for the manipulations in the nature and number of non-covalent interactions in **1**-**3** and **7**. The diversified supramolecular architectures of **1**-**3** and **7**, essentially caused by *para*-substituents of peripheral phenyl rings can be described as follows.

4,4'-bis(benzylideneamino)diphenyl ether [$C_{26}H_{20}N_2O$] (1)

Compound **1** crystallizes in centrosymmetric monoclinic $P2_1/n$ space group and the oxygen atom (O1) sits on a special position. The X-ray crystal structure of **1** show a half of the molecule of [$C_{26}H_{20}N_2O$] in its asymmetric unit and complete molecule is generated through symmetry operation is shown in figure 2(a). There are four such units in the unit cell. The relevant parameters are tabulated in Table 4. The selected bond distance (Å) and bond angle (°) for **1** are: O(1)-C(11) 1.381(4), O(1)-C(14) 1.388(4), N(1)-C(7) 1.266(4), N(2)-C(20) 1.274(4), N(2)-C(17) 1.411(4), N(1)-C(8) 1.418(4) and C(7)-N(1)-C(8) 121.7(3), C(20)-N(2)-C(17) 121.5(3), N(1)-C(7)-C(4) 122.0(3), N(2)-C(20)-C(21) 121.8(3)°, respectively. The ethereal bond angle C(11)-O(1)-C(14) of 121.5(2)° for **1** (and for **2** 121.0(2)° and **7** 120.3(2)°) is significantly larger than that was observed for **3**, however the ethereal bond angle is comparable with the ethereal bond angle observed for N,N'-Bis[(E)-2-thienylmethylene]-4,4'-oxydianiline.[24] The other parameters are found to be in the normal range and have a good agreement with those observed for the similar compounds and reported in earlier literatures.[24,25,26]

Interestingly, compound **1** containing *p*-H positioned on peripheral phenyl rings adopts such a conformation that is thermodynamically stabilized *via* intermolecular CH...π interactions. The central phenyl rings are in anti-parallel orientation, adopting *'gauche'* conformation with dihedral angle of 59.79°, required for the pragmatic CH...π interactions. For such interactions to occur, it is not necessary that the hydrogen atom should be positioned directly above the phenyl ring plane. It may be slightly offset outside the ring as it is seen in our case and in others.[27]

In the crystal packing, each molecule forms two acceptors and two donors CH...π interactions involving central phenyl rings leading to a supramolecular unit consist of five molecules aggregate as shown in figure 2(b). In this unit, the central molecule is sandwiched between two sets of two parallel molecules where the connecting phenyl rings form a dihedral angle of 65.64°. Of more interesting, these supramolecular units can be used to generate 2D infinite channels (~ 4.793 × 5.344 $Å^2$) in the *ab* plane through CH...π interactions as shown in figure 2(c) and 2(d). All H atoms, except those participating in the CH...π contacts were omitted for clarity. In the supramolecular architecture, molecules are arranged in such a way that C15-H15 and C13-H13 groups of central phenyl rings are positioned above to the central phenyl ring

planes of two neighbouring molecules, forming two donors C15-H15...Cg1 (Cg1 = centroid of C8C9C10C11C12C13) and C13-H13...Cg2 (Cg2 = centroid of C14C15C16C17C18C19) interactions. At the same time, central phenyl rings form two acceptor C15-H15...Cg1 and C13-H13...Cg2 interactions, involving C15-H15, C13-H13 groups of other two neighbouring molecules. The distances H15...Cg1 and H13...Cg2 of 2.767 Å and 2.786 Å and favourable α angles (angle between the line connecting Cg, H atom and the normal to the phenyl ring plane as shown in figure 1) of 3.45° and 3.68°, respectively are in the standard range. The first α angle was calculated from α = 90°-θ where θ is the angle of intersection of the phenyl ring plane and the other plane drawn through H15, C9, C12 whereas the second α angle was obtained in a similar way using phenyl ring plane and the plane drawn through H13, C16, C19. The β angles C15-H15···Cg1 and C13-H13···Cg2 of 137.03° and 137.91° are large enough to facilitate these interactions.

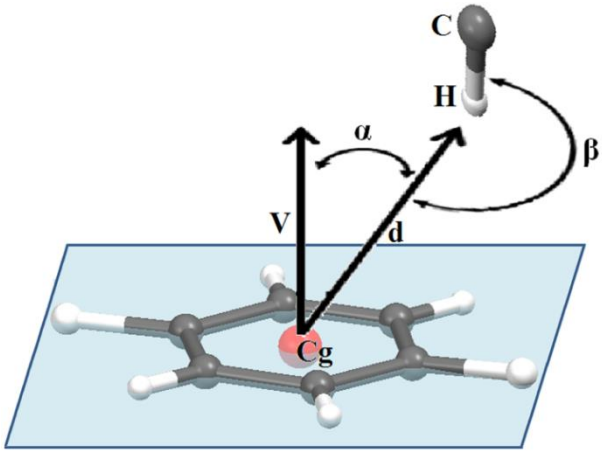

Figure 1. Protocol for CH...π interactions: d is the distance between the phenyl ring centroid (Cg) and the H atom; V is the vector normal to the plane of phenyl ring; α is the angle between the d and V vector, and β is the C–H...Cg angle.

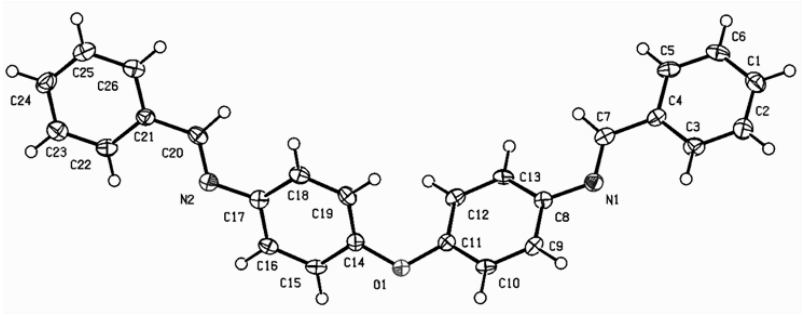

(a)

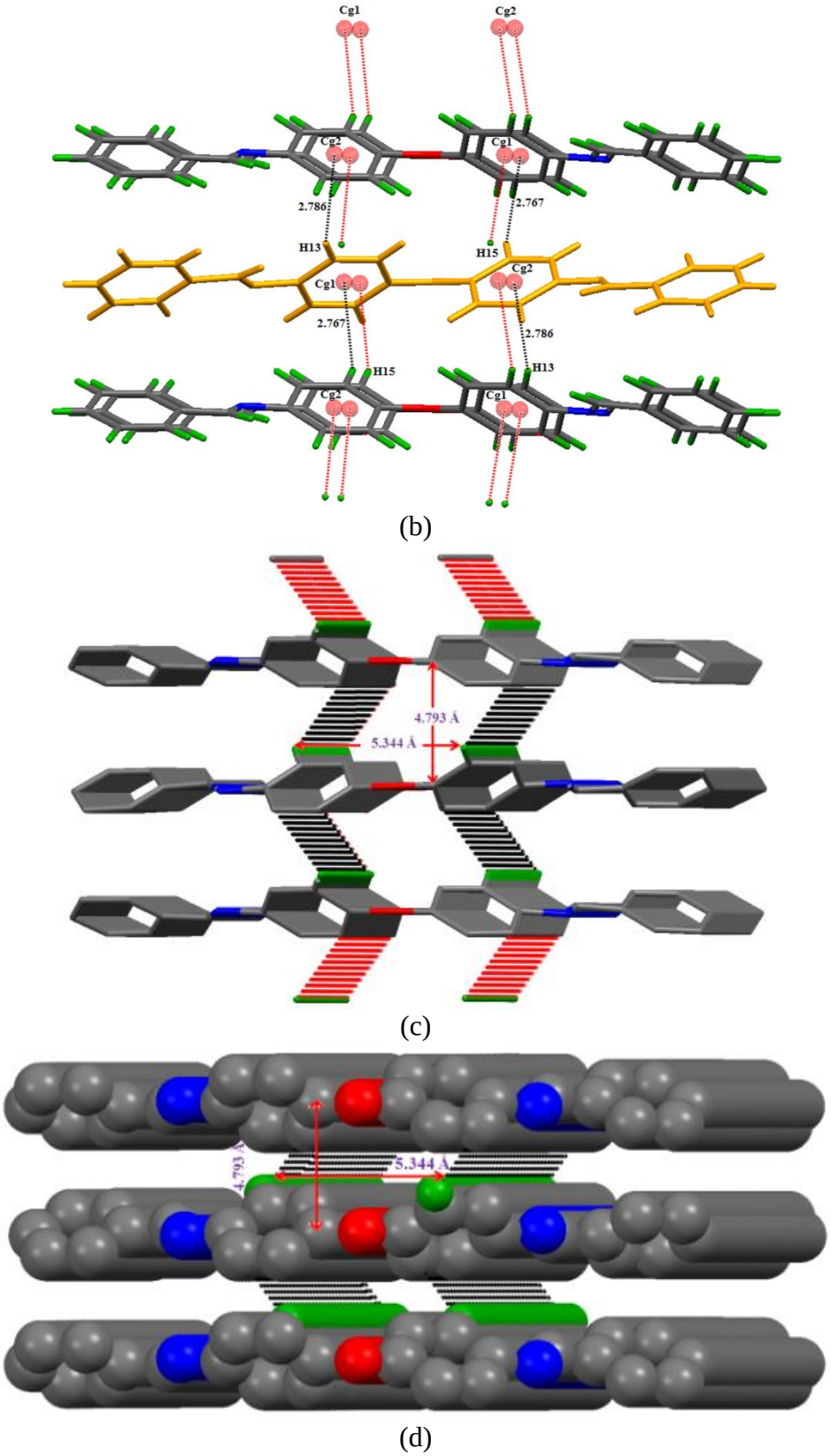

Figure 2. (a) Thermal ellipsoidal plot of compound **1** with atom labeling scheme; (b) Supramolecular unit consists of five molecule aggregates involving CH...π interactions; (c) Formation of supramolecular 2D infinite channels (~ 4.793 × 5.344 Å^2) in the *ab* plane; (d) Space filling representation of 2D non-classical hydrogen bonding network in **1** (all H atoms except those participating in the CH...π contacts were omitted for clarity).

4,4'-bis(p-methoxybenzylideneamino)diphenyl ether [$C_{28}H_{24}N_2O_3$] (2)

Compound **2** crystallizes in the centrosymmetric orthorhombic *C*2cb space group and the oxygen atom (O1) sits on a special position. The X-ray crystal structure of compound **2** shows a half of the molecule of [$C_{28}H_{24}N_2O_3$] in its asymmetric unit and a complete molecule is generated through symmetry operation is shown in figure 3(a). There are four such units in the unit cell. The relevant parameters are tabulated in Table 4. The selected bond distance (Å) and bond angle (°) for **2** are: O(1)-C(1) 1.387(3), O(1)-C(1)# 1.387(3), N(1)-C(4) 1.422(3), N(1)-C(7) 1.258(3), C(7)-C(8) 1.469(4) and C(1)#1-O(1)-C(1), 121.0(3), C(4)- N(1)-C(7), 121.4(2), N(1)-C(7)-C(8), 122.3(3), respectively. These values were found in the normal range (*vide supra*).

Of more fascinating, the *p*-OCH_3 positioned on each of the peripheral rings is capable of having a large enough effect on the crystal packing of **2**, for instance, the introduction of *p*-OCH_3 substituents on the peripheral rings automatically increase the intermolecular distance between the molecules in the solid state, leading to the switching off the typical CH...π synthons (Figure 3(b)) seen in **1** and later in **7**. Further *p*-OCH_3 substituents tend to favour CH...O interactions involving C14-H14B...O2 donor-acceptor contacts. It can freely rotate to meet the stereochemical requirements for self-assembly and to give rise to a '2D' molecular network consisting of alternately **P** and **M** helices. Hence, CH...π stacking becomes increasingly unlikely which ultimately switches off the CH...π interactions. In fact, each -OCH_3 groups form two C14-H14B...O2 donor-acceptor contacts and link two molecules along the *b*-axis with the H14B···O2 distance of 2.574 Å which is in good agreement with the similar interactions reported in literature [12]. Interestingly, the C14-H14B...O2 donor-acceptor groups of the linked molecules connect another set of two molecules along *a*-axis in a trans manner and thereby aligned the incoming molecules parallel to the previous set of two molecules along a-axis with intermolecular spacing of ~ 3.087Å.

As a result of these stimulating interactions, CH...O contacts automatically move towards a helical type, arranged the molecules into attractive 2D sheet with vertically aligned helices bearing internal racemate in the *ab* plane as shown in figure 3(d). Since the assembly is composed of both P and M helices (centric space group) generated by CH...O contacts, the overall molecular packing is achiral, affording thus an internal *racemate*. This tendency of -OCH_3 group of **2** to favour helical contacts is

unprecedented. However, -OCH_3 groups are known to favour reciprocal contacts among each other in the crystal structures of methoxy-substituted distryrylbenzenes.[18,28]

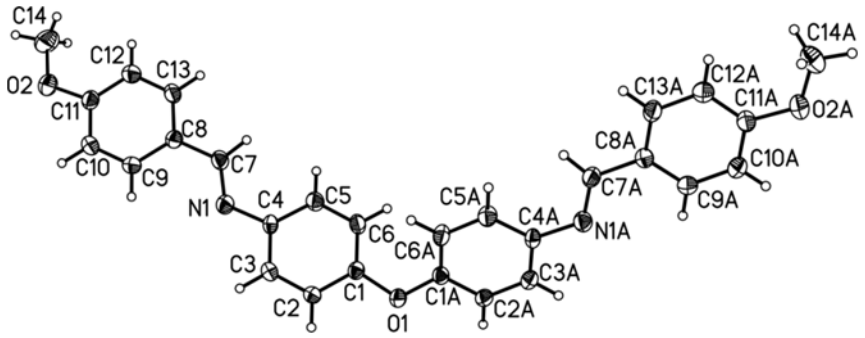

(a)

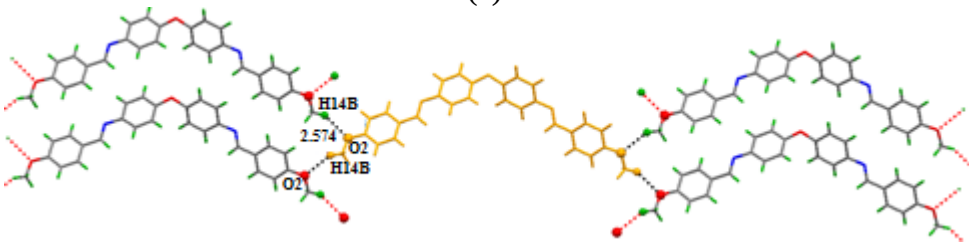

(b)

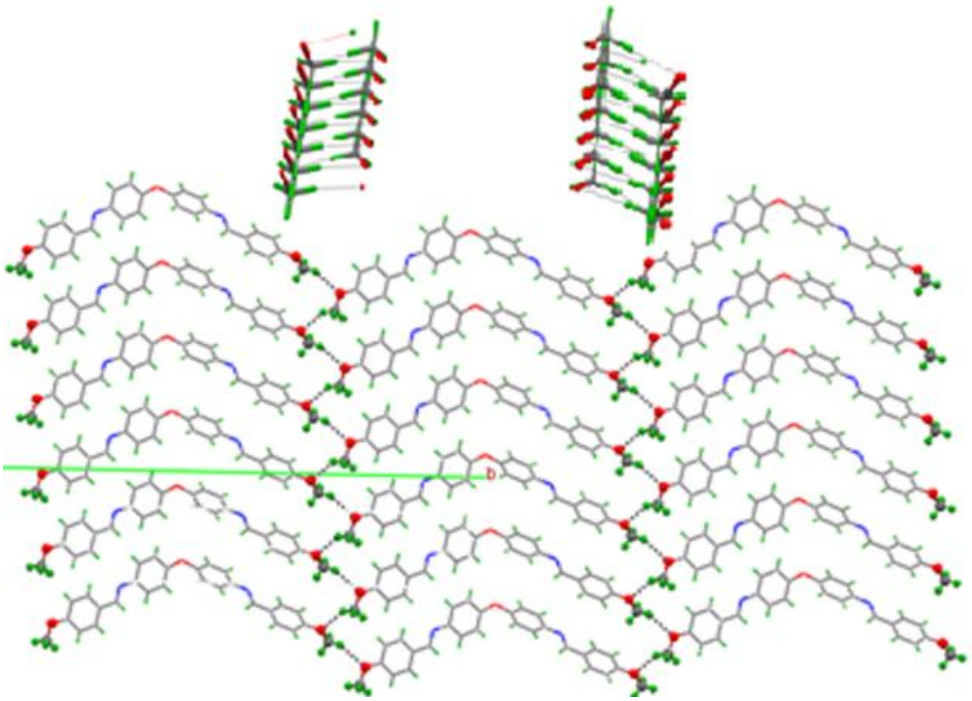

(c)

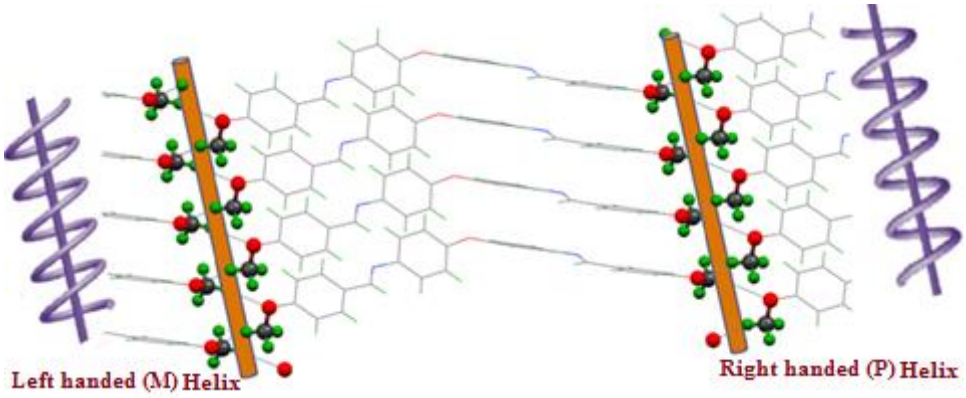

(d)

Figure 3. (a) Thermal ellipsoidal plot of compound **2** with atom labeling scheme (b) supramolecular unit consists of five molecule aggregates involving CH...O interactions (c) CH...O interactions leading to attractive 2D sheets with vertically aligned helices bearing internal racemate in the *ab* plane (d) CH...O induced left-handed and right-handed helices in **2**.

4,4'-bis(p-nitrobenzylideneamino)diphenyl ether [$C_{26}H_{18}N_4O_5$] (3)

A compound **3** crystallizes in a triclinic P-1 space group and the oxygen atom (O1) sits on a special position. The X-ray crystal structure of compound **3** shows a half of the molecule of [$C_{26}H_{18}N_4O_5$] in its asymmetric unit and complete molecule is generated through symmetry operation is shown in figure 4 (a). There are two such units in the unit cell. The relevant parameters are tabulated in Table 4. The selected bond distance (Å) and bond angle (°) for **3** are: O(3)-C(14) 1.3863(19), O(3)-C(11) 1.3869(18), N(2)-C(7) 1.2605(19), N(2)-C(8) 1.4193(19), N(1)-C(1) 1.471(2), O(1)-N(1) 1.208(2), O(2)-N(1) 1.2167(19), C(11)-O(3)-C(14) 118.89(13), C(7)-N(2)-C(8) 118.51(15), C(20)-N(3)-C(17) 120.96(17), O(1)-N(1)-O(2), 123.03(16) and O(5)-N(4)-O(4) 123.17(19), respectively.

More excitingly, the introduction of *p*-NO_2 substituents on each of the peripheral rings increases the dihedral angle between two central phenyl rings bonded to the ethereal oxygen, drastically from 59.79° (observed in **1**) to 75.70°. Further, the deviation from the co-planarity of -NO_2 groups with the peripheral phenyl rings to which they are attached, making a dihedral angles 3.64 (N1-O1-O2) and 6.16 (N4-O4-O5), increases the flexibility of this compound and thus increases the number of intermolecular contacts leading to a fascinating 3D supramolecular architecture. Because of favoured CH...O, CH...N, π...π interactions, weak CH...π interaction becomes unlikely and thus switching off the possibility of the CH...π interactions in **3**. Hence, the molecule present in the unit cell possesses a number of intermolecular contacts. Half of the molecule present at one side of the ethereal oxygen is involved in two π...π, one C25-H25...N2 donor and one C12-H12...O4 acceptor interactions only

whereas the half of the molecule present at the other side of the ethereal oxygen, is involved in two C7-H7...O1 and C13-H13...O2, donor-acceptor interactions along with one C12-H12...O4 donor and one C25-H25...N2 acceptor interactions. As a result, the supramolecular unit consists of seven molecules aggregate as shown in figure 4(b). Moreover, each molecule forms indeed a pair of four closing contacts with four neighbouring molecules (a part of it is shown in figure4 (c)). First two closing contacts involving two donor-acceptor interactions H13...O2 (2.720 Å) and H12...O4 (2.548 Å) forming cavities of dimensions ~ 3.481 × 11.644 $Å^2$ and ~ 2.396 × 15.849 $Å^2$, respectively which are arranged in a *zigzag* pattern (Figure 4(c)). The third closing contact involves a pair of π···π interactions with the Cg1···Cg2 distances of 3.782 Å (Centroid Cg1 = C14 C19 C18 C17 C16 C15; Cg2 = C22 C23 C21 C24 C25 C26) forming a cavity of dimension ~ 3.782 × 6.413 $Å^2$, which is placed above the cavity generated through H12···O4 interactions. However the fourth one involves a pair of H25...N2 (2.615 Å) donor-acceptor contacts forming a cavity of dimension ~ 4.802 × 13.405 $Å^2$, exactly along *b*-axis, which is orthogonal to cavity generated through π···π interactions along *a*-axis. As mentioned above, among all the five types of donor-acceptor contacts H12...O4, H13...O2, H7...O1, Cg1...Cg2 and H25...N2, the four are involved in close contacts with four neighbouring molecules whereas the fifth H7...O1 donor-acceptor interactions of each molecule connect another two molecules exactly in opposite direction (Figure 4(d)) and provides an opportunity to extend the dimensionality along b-axis. The mutual effect of all these contacts in supramolecular architecture result in the translation of the cavities (*vide supra*) into 3D infinite channels as shown in figure 4(e).

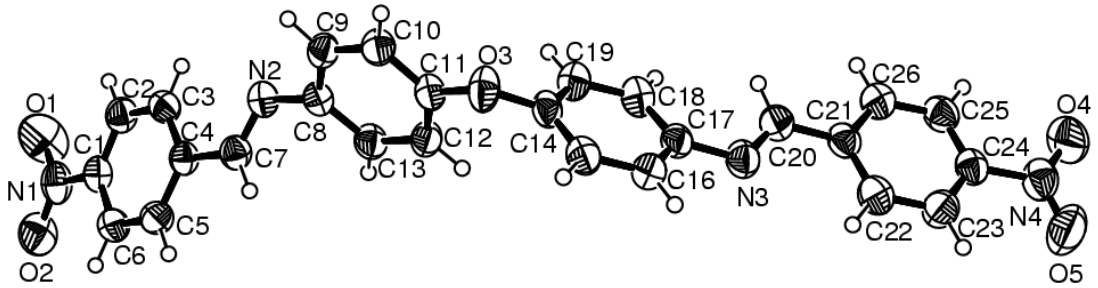

(a)

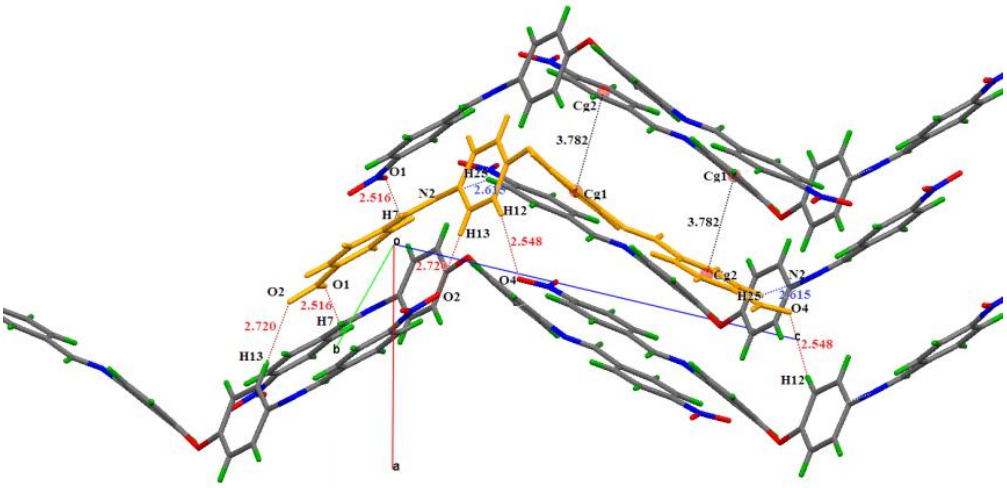
Cg2
3.782
Cg1
O1
H25
2.516
N2
H7
H12
H13
2.548
2.720
O2
O4
2.615
c
a
b

(b)

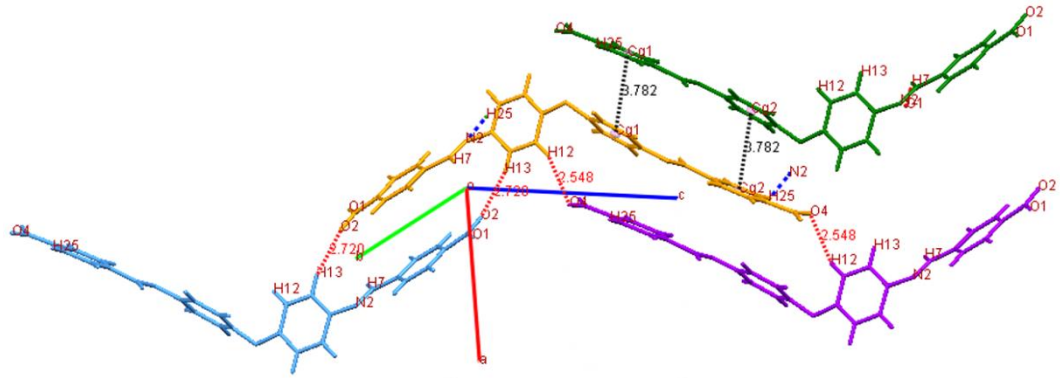
Cg1
3.782
Cg2
H25
H12
H13
H7
N2
O1
O2
O4
2.548
2.720
c
a
b

(c)

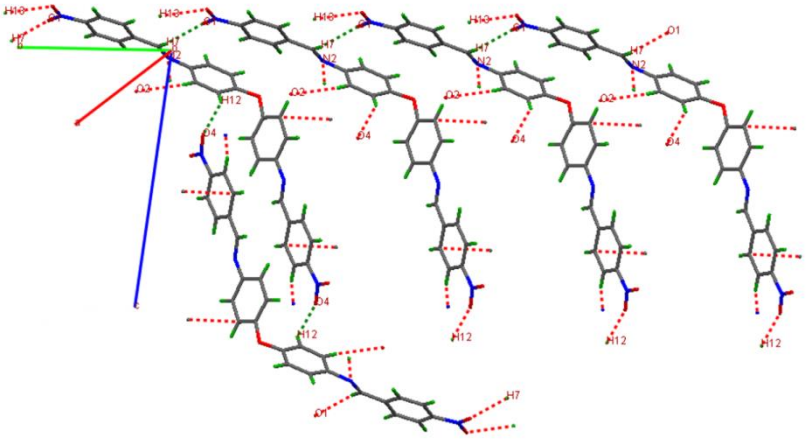

(d)

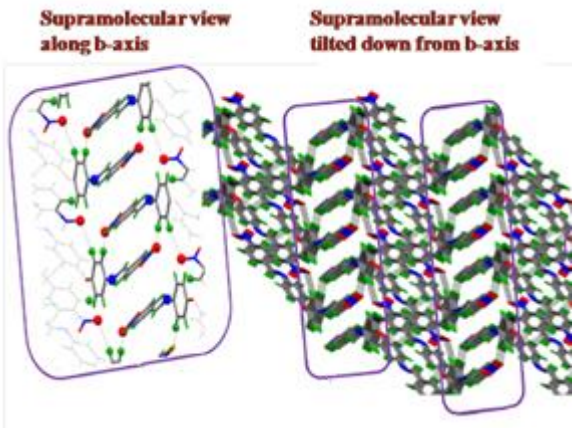

(e)

Figure 4. (a) Thermal ellipsoidal plot of compound **3** with atom labeling scheme; (b) Supramolecular unit consists of seven molecule aggregates involving π...π, CH...O, CH...N hydrogen bonding interactions; (c) Illustration of a part of closing contacts through π...π, CH...O; (d) H7...O1 donor-acceptor interactions extending the dimensionality along b-axis; (e) Formation of 3D supramolecular infinite tunnels.

4,4'-bis(benzylamino)diphenyl ether [$C_{26}H_{24}N_2O$] (7)

This compound crystallizes in the centrosymmetric orthorhombic *P*bna space group and the oxygen atom (O1) sits on a special position. The X-ray crystal structure of compound **7** shows a half of the molecule of [$C_{26}H_{24}N_2O$] in its asymmetric unit and complete molecule is generated through symmetry operation is shown in figure 5(a). There are four such units in the unit cell and the relevant parameters are tabulated in Table 4. The selected bond distance (Å) and bond angle (°) for **7** are: O(1)-C(1) 1.385(2), O(1)-C(1)# 1 1.385(2), N(1)-C(4) 1.397(3), N(1)-C(7) 1.427(3), C(7)-C(8) 1.506(3) and C(1)-O(1)-C(1)# 1 120.3(2), C(4)-N(1)-C(7) 122.5(2), N(1)-C(7)-C(8) 111.3(2), respectively.

The dihedral angle between the least squares planes through the central phenyl rings is 67.20°. The dihedral angle between the least squares plane through one peripheral ring and the plane through the central ring is 74.02° whereas the angle between the plane through the central ring and the plane through other peripheral ring is 74.03° and both of these angles are almost equal. Thus the presence of flexibility in the molecule brings all the aromatic rings in *'gauche'* conformation which is thermodynamically stabilized *via* intermolecular CH...π interactions. It is to be noted that unlike compound **1**, the acidity associated with peripheral phenyl rings appears to dictate the packing motifs through CH...π interactions. In this compound, peripheral phenyls act as donor-acceptor sites for CH...π interactions leading to a supramolecular unit consists of five molecules aggregate as shown in figure 5(b). Evidently, the reduction of **1** to **7** alters the channels like packing patterns of **1** to a wavy like packing

patterns of **7** as shown in figure 5(c). The CH...π interactions in this compound appears to be stronger (α=3.12° and β=153.77°) than in compound **1**, leading to more stable self-assembly. The angle α was calculated from α = 90°-θ where θ is the angle of intersection of the phenyl ring plane and the other drawn through H13, C8, C11. Similar to compound **1**, self-assembly occurs by sandwiching one molecule between two sets of parallel molecules where the connecting phenyl rings make a dihedral angle of 74.92°. In the crystal packing molecules are arranged in such a way that C13-H13 groups of peripheral phenyl rings position above the peripheral phenyl ring plane of two neighbouring molecules, forming two donors C15-H15...Cg (Cg = centroid of C8C9C10C11C12C13) interactions. These interactions connect two molecules, one above and one below to the centrosymmetric molecule in a wavy pattern as shown in figure 5(b). At the same time, peripheral phenyl rings form two acceptors C13-H13...Cg (Cg = centroid of C8C9C10C11C12C13) interactions, linking another two set of molecules, each aligned parallel to the previously connected molecules and sandwiching the centrosymmetric molecule. These intermolecular interactions lead to the arrangement of molecules into supramolecular 2D sheet as shown in figure 5(d). The structural parameters for these interactions are summarized in table 5.

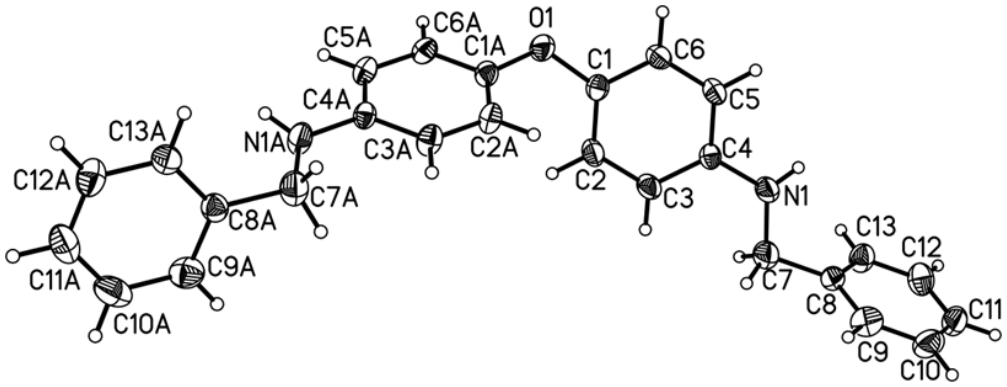

(a)

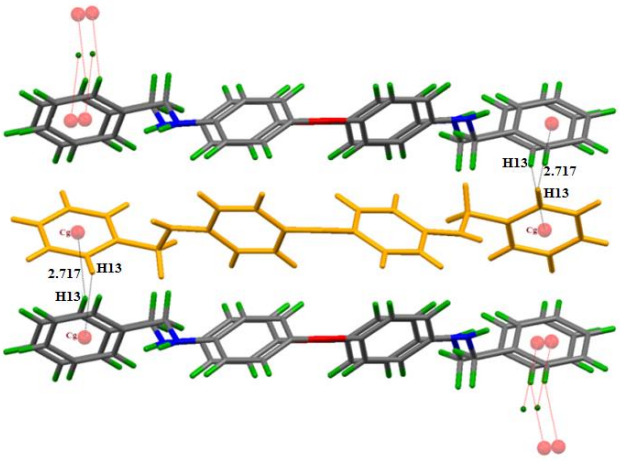

(b)

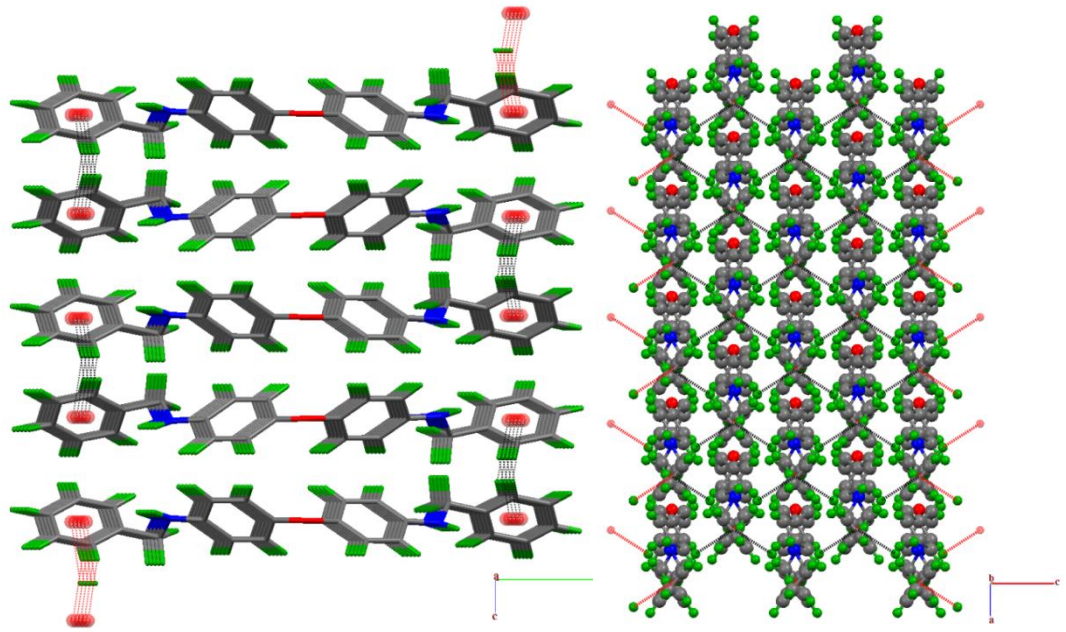

(c) (d)

Figure 5. (a) Thermal ellipsoidal plot of compound **7** with atom labeling scheme; (b) Supramolecular unit consists of five molecule aggregates involving CH...π interactions; (c) Wavy arrangement of molecules of **7** through CH...π interactions; (d) View of molecular packing along *b*-axis.

5A.3.4 Biological importance: *In vitro* cytotoxic activity

The polyaromatic hydrocarbons have been considered as one of the robust antitumor agents due to their efficient intercalating ability leading to the higher cytotoxic activity. For instance, the biological evaluations of polyaromatic compounds such as chrysene and 1-pyrene methylamine derivatives have been reported by Becker and co-workers.[29] These compounds have been shown to possess a broad spectrum of chemotherapeutic activity against both murine and human tumors and in some case these were chosen for clinical development. Recently, a new class of compounds has been reported[30] as polyaromatic substituted podophyllotoxin congeners.[31] These have been proven promising structures for the development of new anticancer agents for human cancer cell lines. It appears that *O*-linked (ethers, esters) and *S*-linked (thioethers) compounds are less active in comparison to the *N*-linked congeners.[1,32] Although a primary investigation on *in vivo* mutagenicity of 4,4'-diaminodiphenyl ether and its *N*-acetyl derivative towards Salmonella typhimurium TA98 and TA100 was reported in 1985 by Tanaka et al.,[33] there is no reports on further investigations of biological properties of 4,4'-diaminodiphenyl ether and its derivatives. Moreover, no data are available to assess the mutagenicity or teratogenicity of any derivative of 4,4'-diaminodiphenyl ether to human.

In the light of these aspects, it was pertinent to investigate 4,4'-diaminodiphenyl ether derivatives for their potential uses from the biological and medicinal points of view. Hence, compounds **1, 4-7, 9-10** (**entry 1-7**) and leader compound **L** was evaluated for their cytotoxic activity by the MTT assay[34] against two malignant tumor cell lines: HEP 3B and IMR 32 and the cytotoxicity were compared with clinically used antineoplastic drug cisplatin (**R**) (Figure 6). The 50% inhibition concentration (IC_{50}) values obtained after incubation of 6 h for all the compounds against both the cell lines are summarized in Table 5.

Table 5. Cytotoxicity IC_{50} values for compound under investigation against HEP 3B and IMR 32 cancer cells.

Entry	Cytotoxicity IC_{50} (μg/mL)±SE	
	HEP 3B	**IMR 32**
4,4'-diaminodiphenyl ether (**L**)	83.18±0.43	54.55±0.48
4,4'-bis(benzylideneamino)diphenyl ether **(1)**	29.84±0.86	42.95±0.59
4,4'-bis(1-naphthylmethylideneamino)diphenyl ether **(4)**	14.13±0.39	33.5±0.23
4,4'-bis(9-anthracenylmethylideneamino)diphenyl ether **(5)**	59.57±1.99	50.35±0.68
4,4'-bis(9-phenanthrenylmethylideneamino)diphenyl ether **(6)**	44.67±0.84	63.1±1.14
4,4'-bis(benzylamino)diphenyl ether **(7)**	28.18±1.38	31.92±0.91
4,4'-bis(1-naphthylmethylamino)diphenyl ether **(9)**	89.13±2.11	89.13±0.93
4,4'-bis(9-anthracenylmethylamino)diphenyl ether **(10)**	50.12±1.58	65.01±0.55
Cisplatin (**R**)	22.39±0.38	32.36±0.09

The analysis of the IC_{50} values suggests that activity of all the compounds enhanced significantly against both malignant tumor cell lines HEP 3B and IMR 32 after derivatization, except **9** which shows lower activity and is not satisfactory as antitumourogenic compound (Figure 6). Interestingly bisimine **4** and diamine **7** were found extremely active against both HEP 3B (IC_{50}=14.13±0.39) and IMR 32 (IC_{50}=31.92±0.91) cell lines respectively and the data suggests that these compounds proved to be more potent as cytotoxic agents than the clinically used antineoplastic drug cisplatin whose IC_{50} values for HEP 3B and IMR 32 are 22.39±0.38 and 32.36±0.09 respectively. Thus, compound **4** is able to significantly arrest the cell proliferation in HEP 3B cell line however its antiproliferative activity (IC_{50}=33.5±0.23) against IMR 32 cell line is found to be comparable with standard cisplatin (IC_{50}=32.36±0.09). In general all compounds present better activities against HEP 3B as compared to the activities against IMR 32, except **5** which show better activity against IMR 32. One of the reasons for the enhanced cytotoxic activity of **1, 4-7** and **10** compared to the leader compound **L** could be the increased lipophilicity and extended π-conjugation of these compounds bearing polyaromatic substiuents at peripheral positions, which probably facilitate the stacking interaction of these compounds with the biological targets.[35] We have made an effort to establish a correlation between the

observed cytotoxicity of these compounds with the gradual increase in the ring of polyaromatic substituents present on peripheral positions. It appears that the IC_{50} of bisimine compounds gradually decreases and thus cytotoxicity increases against both the cell lines, as the number of aromatic rings in arylmethylidene substituents increases up to 2 (compound **1** and **4**), however a further increase in aromatic fused rings could not preserve the cytotoxic activity, instead it decreases remarkably (compound **5** and **6**). The presence of bulkier substituents might create barriers for permeability through the cellular membrane; hence less availability of the compound at the site of action could be one of the reasons for the decrease in the cytotoxic activity of **5** and **6**. Similar trends could not be observed in case of diamines **7, 9-10** (Figure 7).

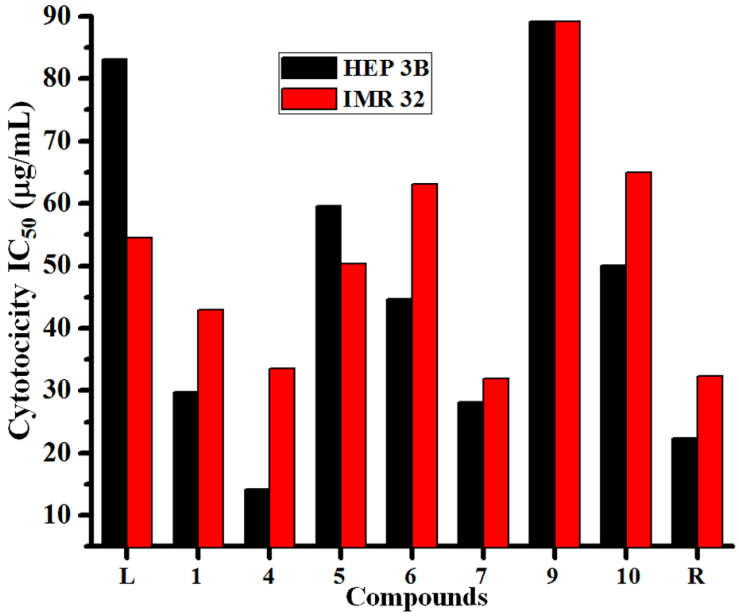

Figure 6. Cytotoxicity IC_{50} (µg/mL) values for compounds **L**, **1**, **4-7**, **9-10** and **R**.

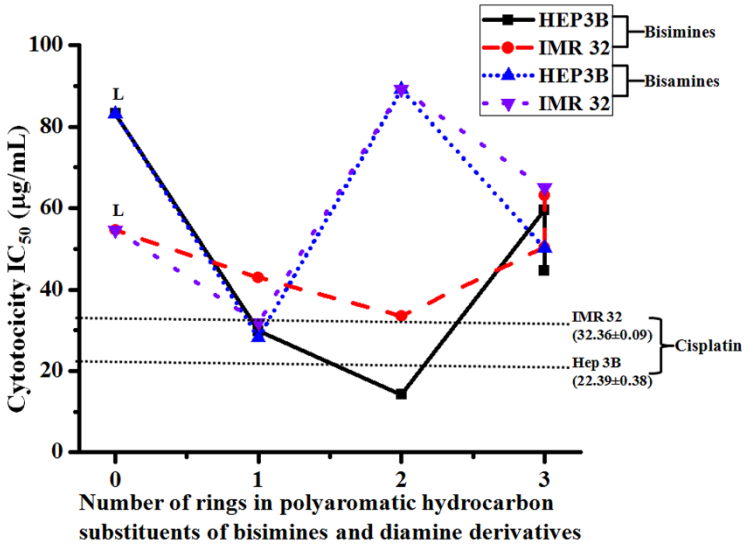

Figure 7. Impact of the change in the size of polyaromatic hydrocarbon substituents of bisimines and diamine derivatives of **L** on cytotoxicity.

Since compound **4** had a remarkable activity against both tested human cancer cell lines, especially the optimum activity against HEP 3B cell line, it was selected for further investigation regarding its mechanism of action. Thus, morphological investigations were carried out by using microscopic photographs of both the cell lines HEP 3B and IMR 32 upon 6 h exposure to the compound **4** and standard cisplatin at their respective *in vitro* growth inhibitory IC_{50} concentrations. The microscopic photographs are shown in figure 8, where A and D show normal proliferation of cells without any insult, B and E show effect of cisplatin on cell growth whereas C and F show less proliferation of cells due to the exposure of compound **4**. The study clearly showed the shrinking of cells, a characteristic apoptotic sign,[1] indicating the induction of apoptosis as part of the mechanism of action of these compounds. Further to reinforce the hypothesis of involvement of apoptosis in the cytotoxic action of these compounds, we carried out DNA ladder assay[36] (Figure 9) to visualize intra-nucleosomal DNA fragmentation (laddering). DNA fragmentation in the form of a ladder due to endonucleolytic attack is reportedly considered as one of the later steps in the apoptotic process or smearing of DNA due to necrosis. Laddering of DNA clearly suggests that these compounds induce apoptosis in the investigated cells and lead to the cytotoxic activity.

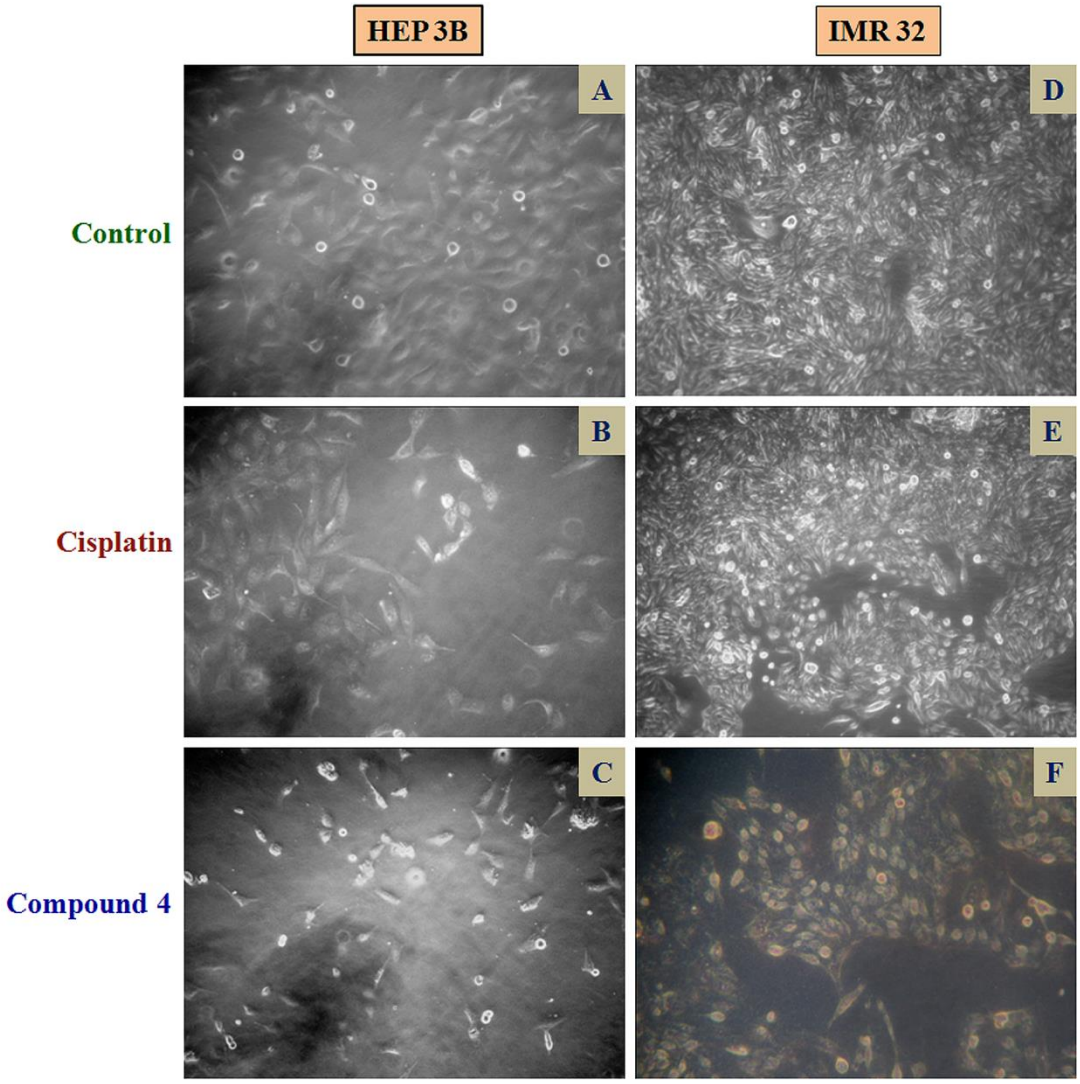

Figure 8. Microscopic photographs of HEP 3B and IMR 32 cells exposed to the cisplatin (middle row) and the compound **4** (lower row) compared to control (top row) indicating the *in vitro* anticancer activity. Compounds were assayed at their respective *in vitro* growth inhibitory IC_{50} value, as determined using the MTT assay in HEP 3B and IMR 32 cells.

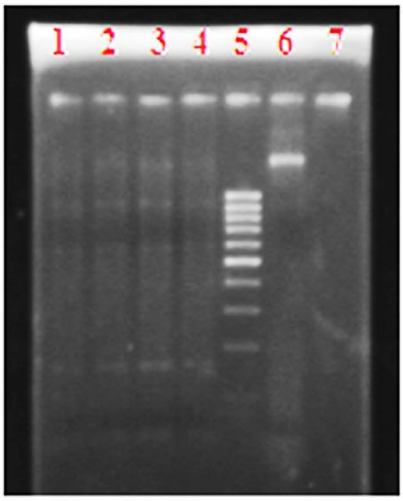

Figure 9. DNA fragmentation assay for compound **4**, **7** and **cisplatin**. (lane 1, 2: compound **7**; lane 3, 4: compound **4;** lane **5**: marker; lane 6, **7**: **cisplatin** at the concentration of their respective IC_{50} values).

5A.4. Conclusions

With intention to study the impact of the incorporation of different polyaromatic hydrocarbon substituents and bisimine/ diamine functionalities on crystal packing and cytotoxicity, we have derivatize 4,4'-diaminodiphenyl ether to obtained a novel series of 4,4'-bis(arylmethylideneamino)diphenyl ethers **1-6** and 4,4'-bis(arylmethylamino)diphenyl ethers **7-10**. All the compounds are well characterized by microanalysis, standard spectroscopic methods and by TGA/DTA analysis. The study allows us to conclude that, the manipulation of *para*-substituents at the peripheral phenyl rings greatly affects the crystal packing patterns and the noncovalent interactions. Compounds **1-3** and **7** are rich in C–H donors and π acceptors, the introduction of *p*-OCH_3 or *p*-NO_2 at the peripheral phenyl rings in **2** and **3** perturb the crystal packing patterns and switches off the CH...π interactions seen in **1** and **7**. The crystal packing of **2** is dominated by CH···O stacking interactions in a helical manner that leads to attractive 2D sheets with vertically aligned helices bearing internal *racemate* in the *ab* plane. This tendency of -OCH_3 group to favour helical contacts is unprecedented. Compound **3** forms 3D infinite channels using a massive number of weak CH...N, CH...O and π...π interactions. Thus, modification at the *para*-substituents efficiently switches over the dimensionality of the crystal packing in solid state. Furthermore, the leader compound 4,4'-diaminodiphenyl ethers and its derivatives were screened for *in vitro* cytotoxic activity against two malignant human cell lines such as HEP 3B and IMR 32 by the MTT assay. Interestingly, some of the derivatives *viz* **4** and **7** were found remarkably active against both the cell lines and these compounds appeared to be more potent as cytotoxic agents than cisplatin. The DNA fragmentation and microscopic photographs support the induction of apoptosis and explain the mode of action of these derivatives as antitumor agents. Thus, ease of synthesis as well as owing interesting packing patterns and *in vitro* anticancer activity against human HEP 3B (hepatoma) and IMR 32 (neuroblastoma) cell lines, make the present series of bisimine and diamine derivatives as a promising new structures towards crystal engineering and for the development of new anticancer agents.

5A.5. References

1. (a) Zhang, H. Z.; Kasibhatla, S.; Kuemmerle, J.; Kemnitzer, W.; O.-Mason, K.; Qiu, L.; C.-Grundy, C.; Tseng, B.; Drewe, J.; Cai, S. X. *J. Med. Chem.* **2005**, *48*, 5215. (b) Mattson, M. P. *Brain Pathol*. **2000**, *10*, 300.
2. (a) Przybylski, P.; Huczynski, A.; Bejcar, K. G.; Brzezinski B.; Bartl, F. *Curr. Org. Chem*. **2009**, *13*, 124. (b) Kiriy, N.; Bocharova, V.; Kiriy, A.; Stamm, M.; Krebs F.C.; Adler, H.-J. *Chem. Mater*. **2004**, *16*, 4765. (c) Zheng, Y.; Ma, K.; Li, H.; Li, J.; He, J.; Sun, X.; Li R.; Ma, *J. Catal. Lett*. **2009**, *128*, 465.
3. Largeron M.; Fleury, M.-B. *Org. Lett*. **2009**, *11*, 883.
4. (a) O'Meara, J. A.; Gardee, N.; Jung, M.; Ben R. N.; Durst, T. J. *Org. Chem*. **1998**, *63*, 3117. (b) Valot, F.; Fache, F.; Jacquot, R.; Spagnol M.; Lemaire, M. *Tetrahedron Lett*. **1999**, *40*, 3689. (c) Szardening, A. K.; Burkoth, T. S.; Look, G. C.; Campbell, D. A. *J. Org. Chem*. **1996**, *61*, 6720. (d) Chiappe C.; Pieraccini, D. *Green Chem*. **2003**, *5*, 193.
5. Salvatore, R. N.; Yoon, C. H.; Jung, K. W. *Tetrahedron* **2001**, *57*, 7785.
6. Singh, V. K.; Kadu, R.; Roy, H. *Eur. J. Med. Chem.* **2014**, *74*, 552.
7. (a) Ding, Y.; Boone, H. W.; Anderson, J. D.; Padias, A. B.; Hall Jr., H. K. *Macromolecules* **2001**, *34*, 5457. (b) Boone, H. W.; Bruck, M. A.; Bates, R. B.; Padias, A. B.; Hall Jr., H. K. *J. Org. Chem.* **1995**, *60*, 5279. (c) Ledbetter Jr., J. W. *J. Phys. Chem*. **1977**, *81*, 54. (d) Largeron, M.; Fleury, M.-B. *Org. Lett*. **2009**, *11*, 883. (e) Jarrahpour, A.; Ebrahimi, E. *Molecules* **2010**, *15*, 515.
8. Glasstone, S. Trans. Faraday Soc. 33 (1937) 200.
9. (a) Sutor, D. J. *Nature* **1962**, *195*, 68. (b) Sutor, D. J. *J. Chem. Soc*. **1963**, 1105.
10. (a) Gu, Y.; Kar, T.; Scheiner, S. *J. Am. Chem. Soc*. **1999**, *121*, 9411. (b) Derewenda, Z. S.; Lee, L.; Derewenda, U. *J. Mol. Biol*. **1995**, *252*, 248. (c) Desiraju, G. R.; Steiner, T. The Weak Hydrogen Bond: In Structural Chemistry and Biology, Oxford University Press, New York, 2001. (d) Hobza, P.; Havlas, Z. *Chem. Rev*. **2000**, *100*, 4253. (e) Desiraju, G. R. *Acc. Chem. Res*. **1996**, *29*, 441. (f) Taylor, R.; Kennard, O. *J. Am. Chem. Soc*. **1982**, *104*, 5063.
11. (a) Marjo, C. E.; Scudder, M. L.; Craig, D. C.; Bishop, R. *J. Chem. Soc., Perkin Trans. 2* **1997**, 2099. (b) Thalladi, V. R.; Gehrke, A.; Boese, R. *New J. Chem*. **2000**, *24*, 463. (c) Mascal, M. *Chem. Commun.* **1998**, 303. (d) Maly, K. E.; Maris, T.;

Gagnon, E.; Wuest, J. D. *Cryst. Growth Des.* **2006**, *6*, 461. (e) Bosch, E. *Cryst. Growth Des.* **2010**, *10*, 3808.

12. (a) Nishio, M. *CrystEngComm* **2004**, *6*, 130. (b) Nishio, M.; Umezawa, Y.; Honda, K.; Tsuboyama, S.; Suezawa, H. *CrystEngComm* **2009**, *11*, 1757. (c) Takahashi, O.; Kohno, Y.; Nishio, M. *Chem. Rev*. **2010**, *110*, 6049. (d) Nayak, S. K.; Sathishkumar, R.; Guru Row, T. N. *CrystEngComm* **2010**, *12*, 3112. (e) Takahashi, O.; Kohno, Y.; Iwasaki, S.; Saito, K.; Iwaoka, M.; Tomoda, S.; Umezawa, Y.; Tsuboyama, S.; Nishio, M. *Bull. Chem. Soc. Jpn*. **2001**, *74*, 2421. (f) Tewari A. K.; Dubey, R. *Bioorg. Med. Chem*. **2008**, *16*, 126. (g) Kobayashi, Y.; Saigo, K. *J. Am. Chem. Soc*. **2005**, *127*, 15054. (h) Saigo, K.; Kobayashi, Y. *The Chemical Record* **2007**, *7*, 47. (i) Sozzani, P.; Comotti, A.; Bracco, S.; Simonutti, R. *Chem. Commun*. **2004**, 768. (j) Hill, J. P.; Scipioni, R.; Boero, M.; Wakayama, Y.; Akada, M.; Miyazaki, T.; Ariga, K. *Phys. Chem. Chem. Phys*. **2009**, *11*, 6038. (k) Tiekink E. R. T.; Z.-Schpector, J. The Importance of Pi-Interactions in Crystal Engineering: Frontiers in Crystal Engineering, John Wiley & Sons Inc., 2012. (l) Nishio, M. *Phys. Chem. Chem. Phys.* **2011**, *13*, 13873. (m) Nishio, M. *J. Mol. Struct*. **2012**, *1018*, 2.
13. (a) Hunter C. A.; Sanders, J. K. M. *J. Am. Chem. Soc*. **1990**, *112*, 5525. (b) Hunter, C. A. *Chem. Soc. Rev*. **1994**, *23*, 101. (c) Janiak, C. *J. Chem. Soc., Dalton Trans.* **2000**, 3885. (d) Headen, T. F.; Howard, C. A.; Skipper, N. T.; Wilkinson, M. A.; Bowron, D. T.; Soper, A. K.; *J. Am. Chem. Soc*. **2010**, *132*, 5735.
14. (a) Desiraju, G. R. *Science* **1997**, *278*, 404. (b) Harakas, G.; Vu, T.; Knobler, C. B.; Hawthorne, M. F. *J. Am. Chem. Soc*. **1998**, *120*, 6405. (c) Kuduva, S. S.; Craig, D. C.; Nangia, A.; Desiraju, G. R. *J. Am. Chem. Soc*. **1999**, *121*, 1936.
15. Desiraju, G. R. *Acc. Chem. Res*. **1996**, *29*, 441.
16. Desiraju, G. R. *Curr. Opi. Sol. Sta. Mat. Sci.* **1997**, *2*, 451.
17. (a) Hulme, A. T.; Price, S. L.; Tocher, D. A. *J. Am. Chem. Soc*. **2005**, *127*, 1116. (b) Kirchner, M. T.; Bläser, D.; Boese, R. *Chem. Eur. J*. **2010**, *16*, 2131.
18. Collas, A.; Bagrowska, I.; Aleksandrzak, K.; Zeller, M.; Blockhuys, F. *Cryst. Growth Des*. **2011**, *11*, 1299.
19. (a) Nishio, M. *Tetrahedron* **2005**, *36*, 6923. (b) Janiak, C. *J. Chem. Soc., Dalton Trans*. **2000**, 3885. (c) Roesky, H. W. Andruh, M. *Coord. Chem. Rev*. **2003**, *236*,

91. (d) Bhosale, S.; Sisson, A. L.; Sakai N.; Matile, S. *Org. Biomol. Chem*. **2006**, *4*, 3031. (e) Bhayana, B. Wilcox, C. S. *Angew. Chem. Int. Ed*. **2007**, *46*, 6833.

20. P.-García, L.; Amabilino, D. B. *Chem. Soc. Rev*. **2002**, *31*, 342.
21. Oxford Diffraction, CrysAlis PRO, Oxford Diffraction Ltd, Yarnton, England, 2009.
22. Sheldrick, G.M. SHELXTL reference manual: version 5.1, Bruker AXS, Madison, WI, 1997.
23. Sheldrick, G.M. SHELXL-97: program for crystal structure refinement, University of Göttingen, Göttingen, Germany, 1997.
24. Tao, X.; Cui, H. *Acta Cryst*. **2009**, *E65*, o2251.
25. (a) Jarrahpour, A.; Zarei, M. *Molecules* **2007**, *12*, 2364. (b) Taneda, M.; Amimoto, K.; Koyama, H.; Kawato, T. *Org. Biomol. Chem*. **2004**, *2*, 499.
26. (a) Kerckhoffs, J. M. C. A.; Peberdy, J. C.; Meistermann, I.; Childs, L. J.; Isaac, C. J.; Pearmund, C. R.; Reudegger, V.; Khalid, S.; Alcock, N. W.; Hannon, M. J.; Rodger, A. *Dalton Trans*. **2007**, 734. (b) Mehata, P. D.; Sengar, N. P. S.; Subrahmanyam, E. V. S.; Satyanarayana, D. *Indian J. Pharm. Sci*. **2006**, *68*, 103.
27. Suezawa, H.; Yoshida, T.; Hirota, M.; Takahashi, H.; Umezawa, Y.; Honda, K.; Tsuboyama, S.; Nishio, M. *J. Chem. Soc., Perkin Trans*. *2*, **200**1, 2053.
28. Velde, C. M. L. V.; Geise, H. J.; Blockhuys, F. *Cryst. Growth Des*. **2006**, *6*, 241.
29. (a) Bair, K. W.; Tuttle, R. L.; Knick, V. C.; Cory, M.; McKee, D. D. *J. Med. Chem*. **1990**, *33*, 2385. (b) Becker, F. F.; Banik, B. K. *Bioorg. Med. Chem. Lett*. **1998**, *8*, 2877. (c) Bair, K. W.; Andrews, C. W.; Tuttle, R. L.; Knick, V. C.; Cory, M.; Mckee, D. D. *J. Med. Chem.* **1991**, *34*, 1983.
30. Kamal, A.; Kumar, B. A.; Suresh, P.; Agrawal, S. K.; Chashoo, G.; Singh, S. K.; Saxena, A. K. *Bioorg. Med. Chem*. **2010**, *18*, 8493.
31. (a) Kamal, A.; Kumar, B. A.; Arifuddin, M.; Dastidar, S. G.; *Bioorg. Med. Chem*. **2003**, *11*, 5135. (b) Kamal, A.; Gayatri, N. L.; Reddy, D. R.; Reddy, P. S. M. M.; Arifuddin, M.; Dastidar, S. G.; Kondapi, A. K.; Rajkumar, M. *Bioorg. Med. Chem*. **2005**, *13*, 6218. (c) Kamal, A.; Laxman, E.; Khanna, G. B. R.; Reddy, P. S. M. M.; Rehana, T.; Arifuddin, M.; Neelima, K.; Kondapi, A. K.; Dastidar, S. G. *Bioorg. Med. Chem*. **2004**, *12*, 4197. (d) Kamal, A.; Kumar, B. A.; Arifuddin, M.; Dastidar, S. G. *Lett. Drug Design Discov*. **2006**, *3*, 205. (e) Kamal, A.; Azeeza, S.; Bharathi, E. V.; Malik, M. S.; Shetti, R. V. *Mini-Rev. Med. Chem*. **2010**, *10*, 405.

32. (a) Wang, Z.Q.; Kuo, Y.H.; Schnur, D.; Bowen, J.P.; Liu, S.Y.; Han, F.S.; Cheng, Y.-C.; Lee, K.-H. *J. Med. Chem*. **1990**, *33*, 2660. (b) Zhou, X.-M.; Wang, Z.-Q.; Chang, J.-Y.; Chen, H.X.; Cheng, Y.-C.; Lee, K.-H. *J. Med. Chem*. **1991**, *34*, 3346. (c) Xiao, Z.; Xiao, Y.-D.; Feng, J.; Golbraikh, A.; Tropsha, A.; Lee, K.-H. *J. Med. Chem*. **2002**, *45*, 2294. (d) VanVilet, D.S.; Tachibana, Y.; Bastow, K. F.; Huang, E.-S.; Lee, K.-H. *J. Med. Chem*. **2001**, *44*, 1422.

33. Tanaka, K.; Ino, T.; Sawahata, T.; Marui, S.; Igaki, H.; Yashima, H. *Mutat. Res*. **1985**, *143*, 11.

34. Manosroi, J.; Dhumtanom, P.; Manosroi, A. *Cancer Letters* **2006**, *235*, 114.

35. Je, J.-Y.; Cho, Y.-S.; Kim, S.-K. *Bioorg. Med. Chem. Lett*. **2006**, *16*, 2122.

36. Basnakian, A. G.; James, S. J. *Nucleic Acids Res*. **1994**, *22*, 2714.

5A.6. Annexure

5A.6.1 NMR spectra: The NMR spectral data for compound **1-10** is given below in annexure 1-10. The presence of most characteristic signals and signals due to aromatic protons in NMR spectrum along with proper splitting pattern give evidence for the desired molecular structure.

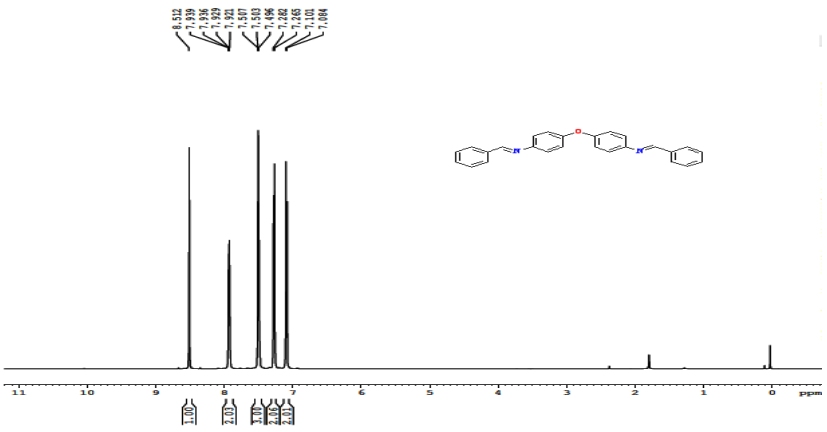

(a)

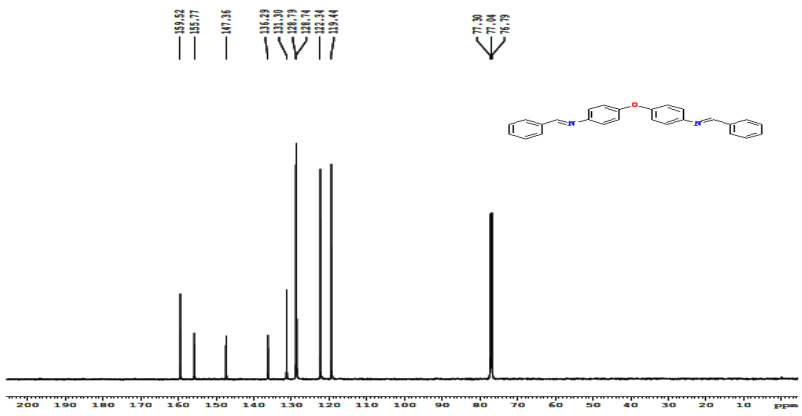

(b)

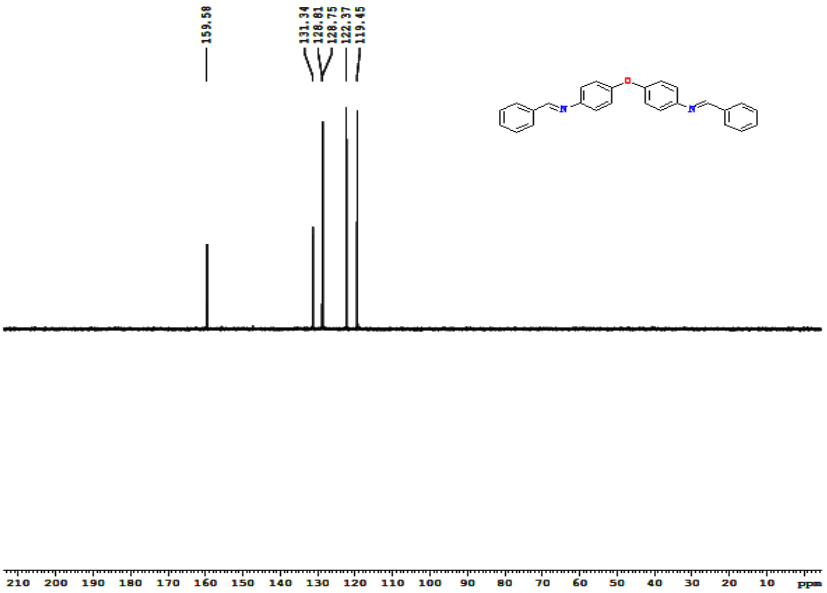

(c)

Annexure 1. NMR Spectral for Compound **1**; (a) ^{1}H NMR spectrum, (b) ^{13}C NMR spectrum, (c) DEPT-135 NMR spectrum.

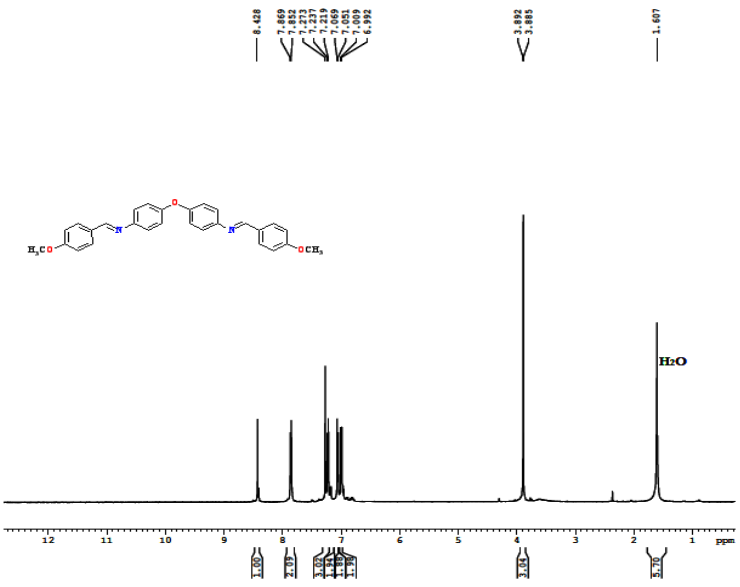

(a)

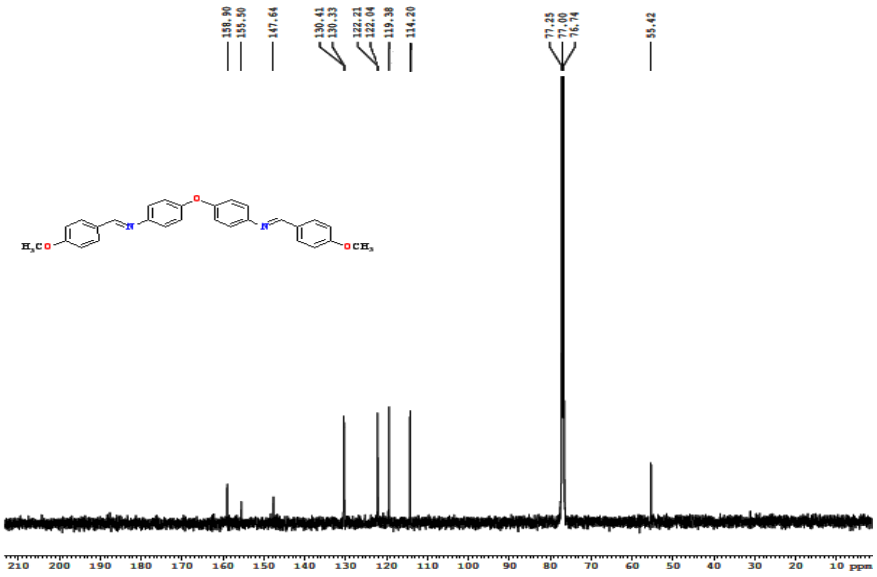

(b)

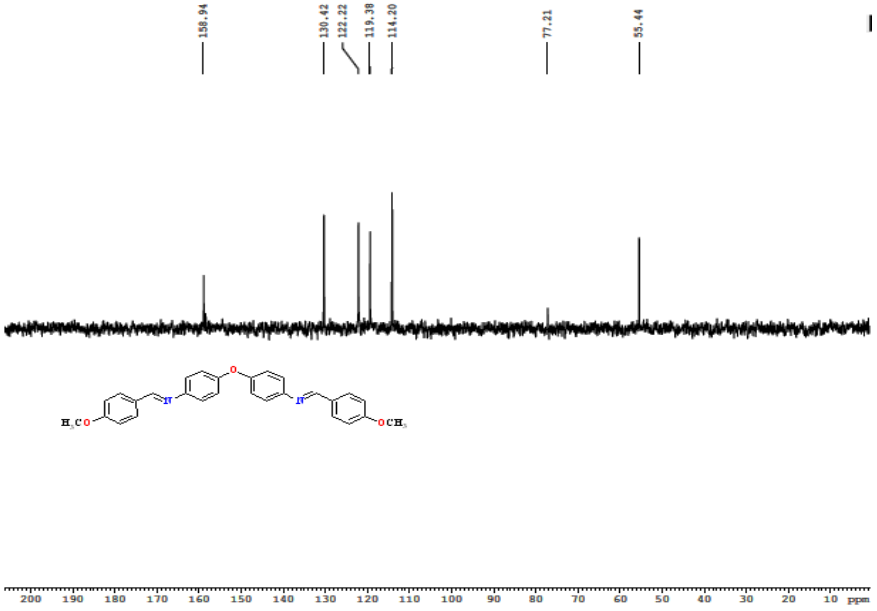

(c)

Annexure 2. NMR spectra for compound **2;** (a) ^{1}H NMR spectrum, (b) ^{13}C NMR spectrum, (c) DEPT-135 NMR spectrum.

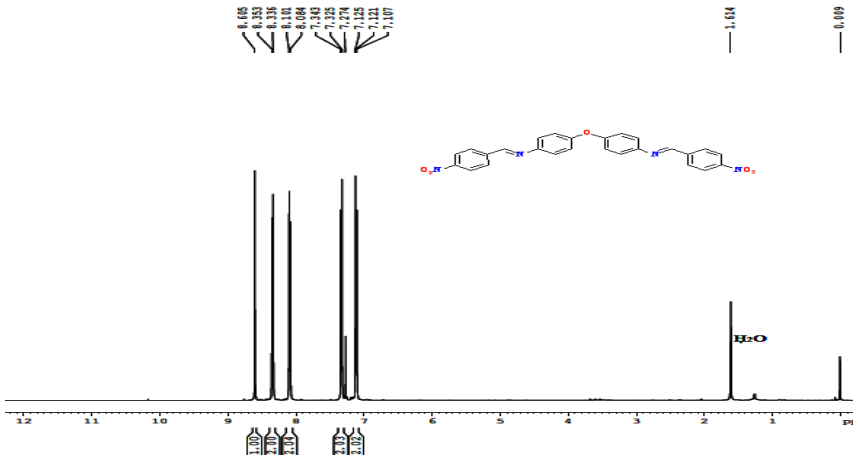

(a)

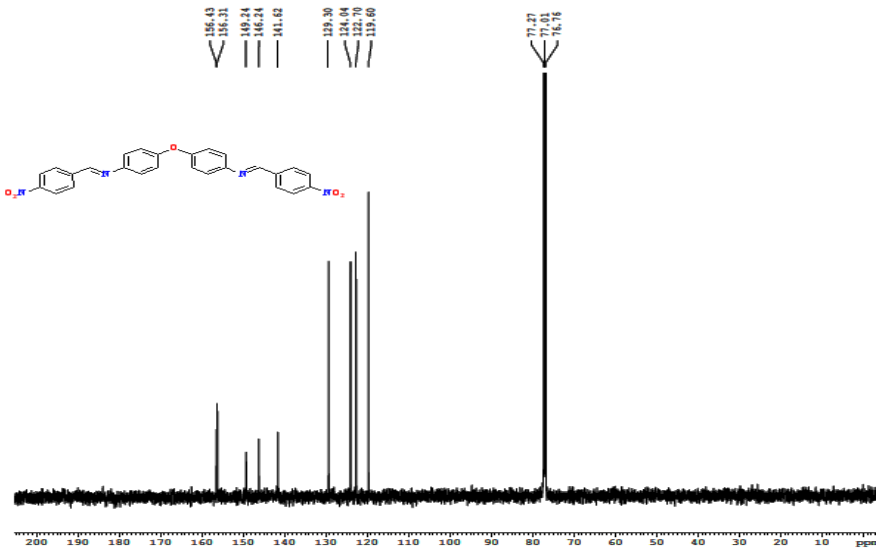

(b)

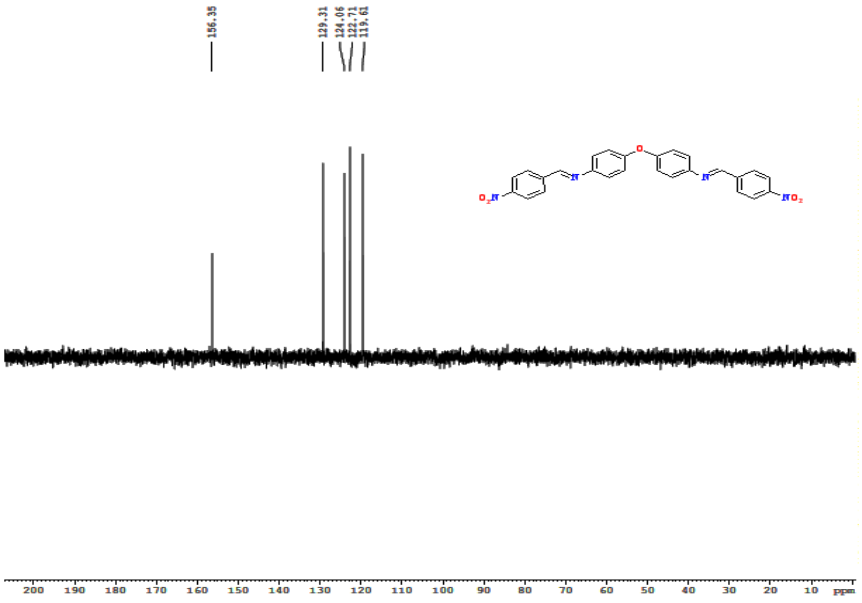

(c)

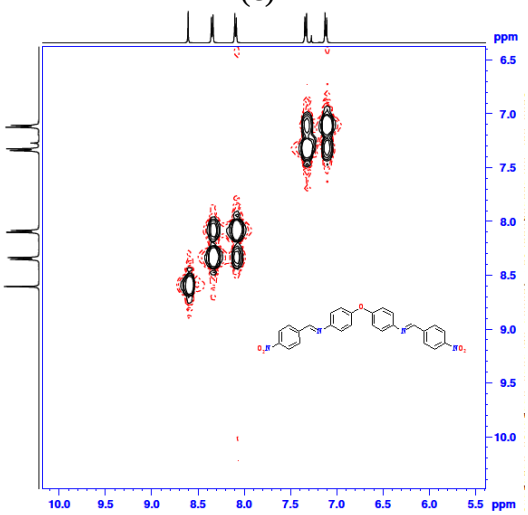

(d)

Annexure 3. NMR spectra for compound **3;** (a) ^{1}H NMR spectrum, (b) ^{13}C NMR spectrum, (c) DEPT-135 NMR spectrum, (d) COSY NMR Experiment.

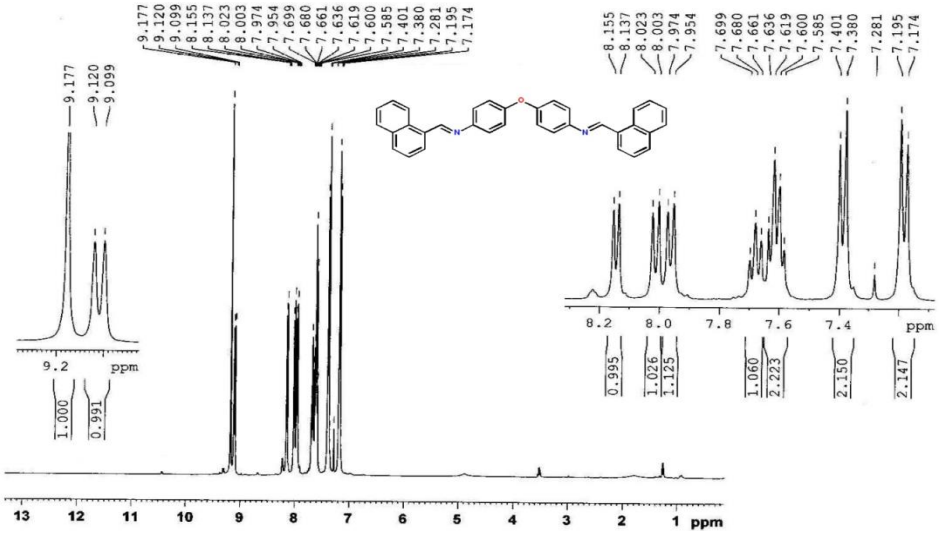
9.177
9.120
9.099
8.155
8.137
8.023
8.003
7.974
7.954
7.699
7.680
7.661
7.636
7.619
7.600
7.585
7.401
7.380
7.281
7.195
7.174
1.000
0.991
0.995
1.026
1.125
1.060
2.223
2.150
2.147
ppm

(a)

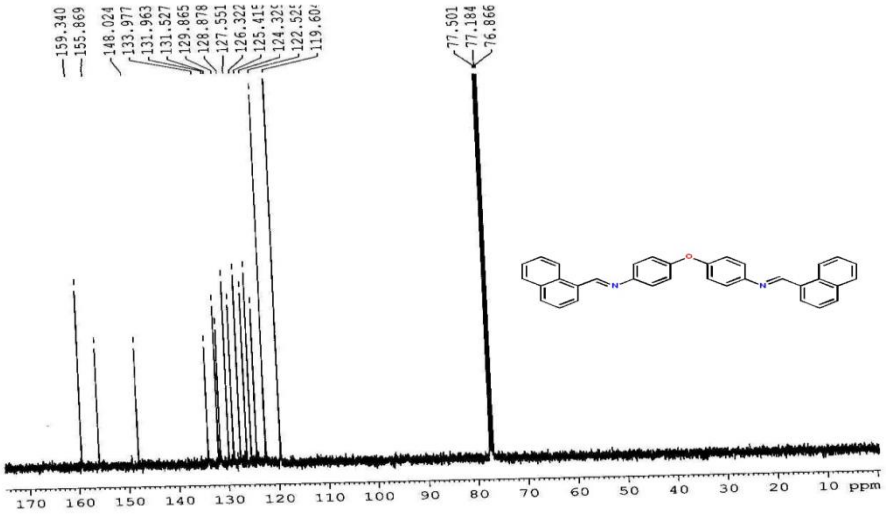
159.340
155.869
148.024
133.977
131.963
131.527
129.865
128.878
127.551
126.322
77.501
77.184
76.866
ppm

(b)

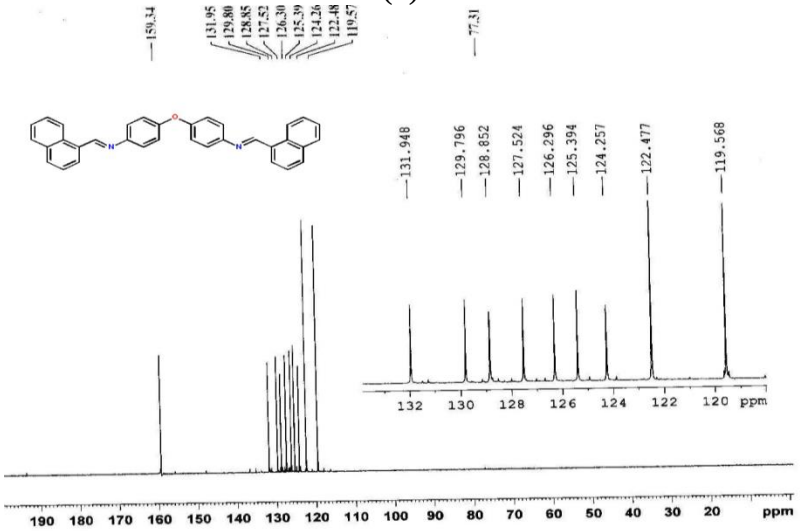
131.948
129.796
128.852
127.524
126.296
125.394
124.257
122.477
119.568
ppm

(c)

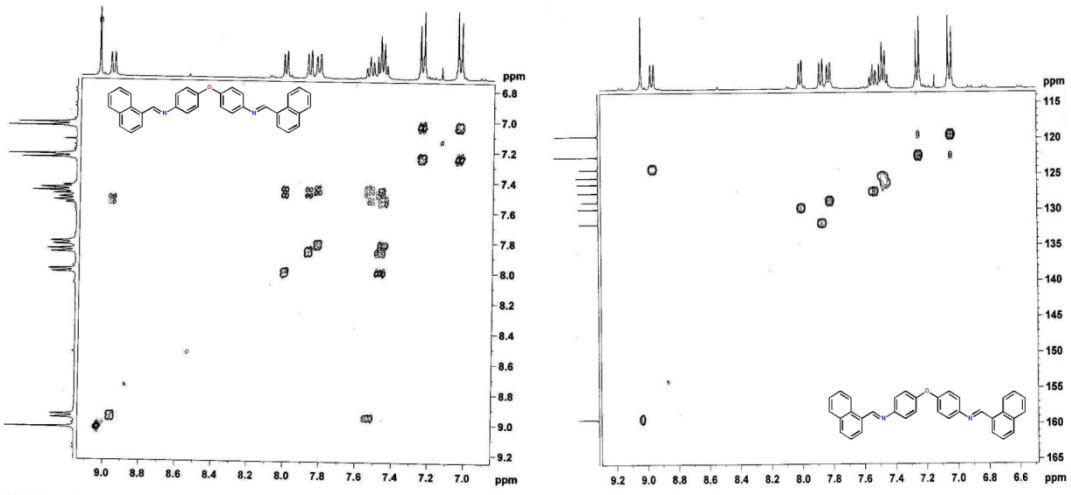

(d) (e)

Annexure 4. NMR spectra for compound **4**; (a) ^{1}H NMR spectrum, (b) ^{13}C NMR spectrum, (c) DEPT-135 NMR spectrum, (d) g-COSY NMR Spectrum, (e) HSQC NMR spectrum.

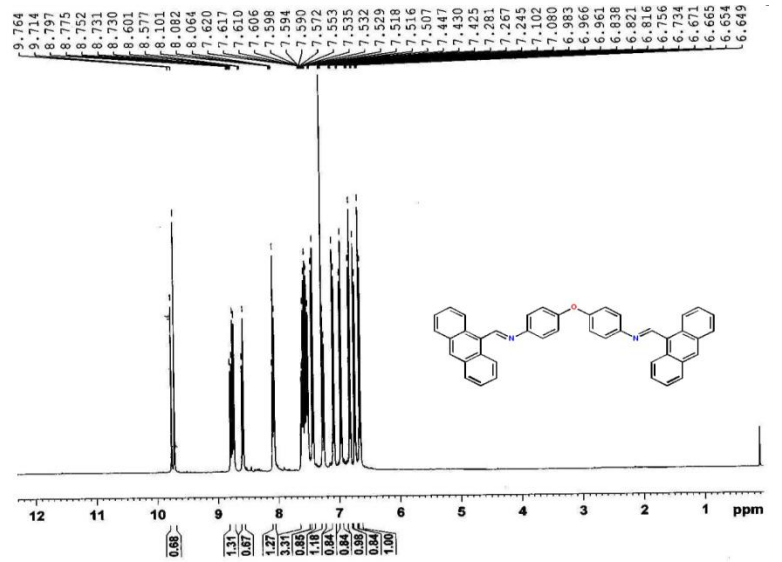

(a)

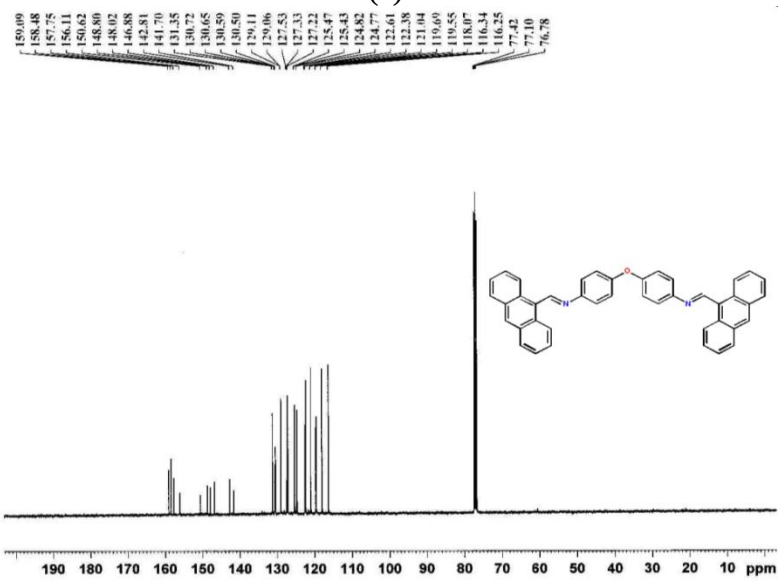

(b)

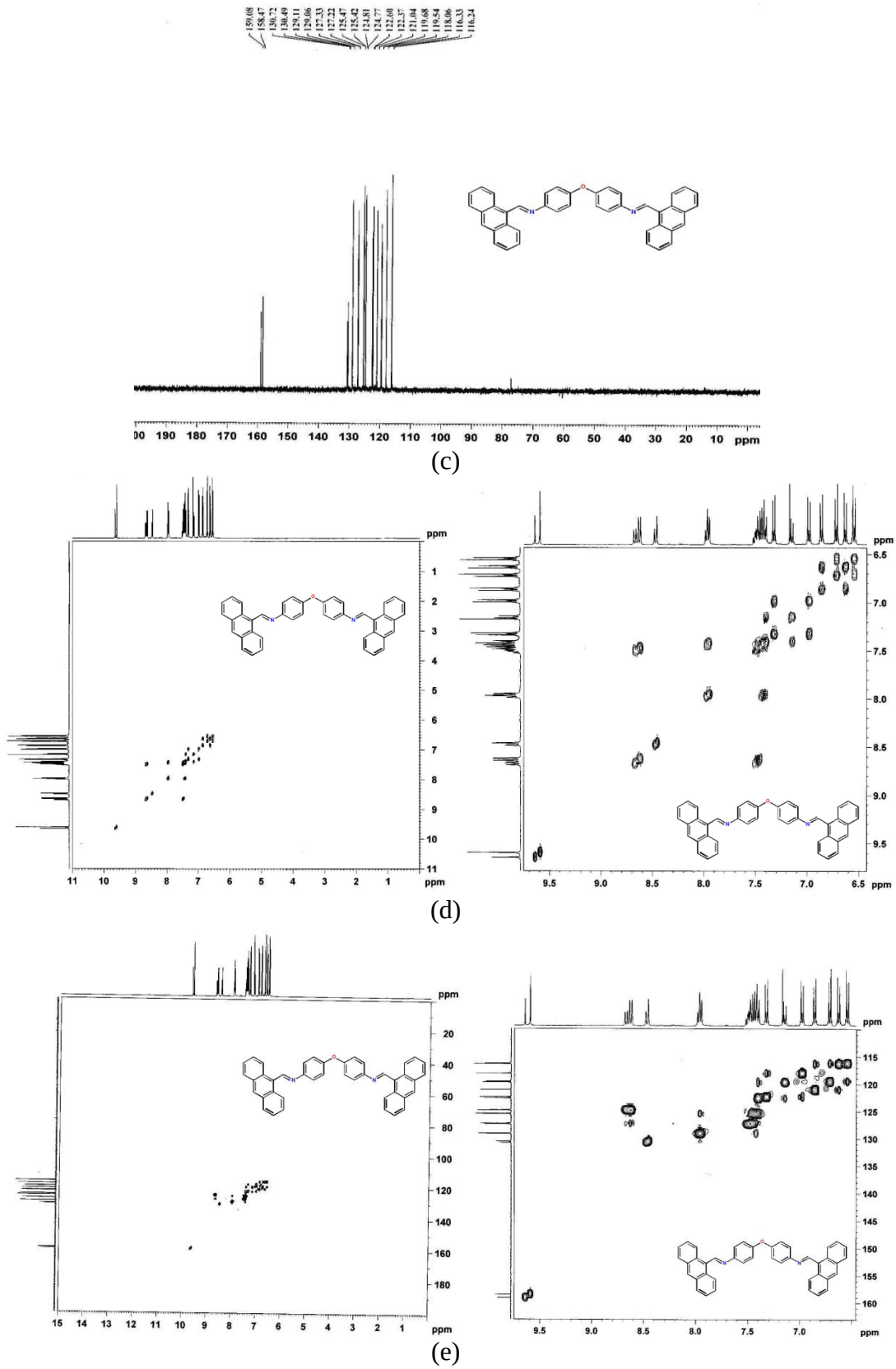

(c)

(d)

(e)

Annexure 5. NMR spectra for compound **5**; (a) ^{1}H NMR spectrum, (b) ^{13}C NMR spectrum, (c) DEPT-135 NMR spectrum, (d) g-COSY NMR Spectrum, (e) HSQC NMR spectrum.

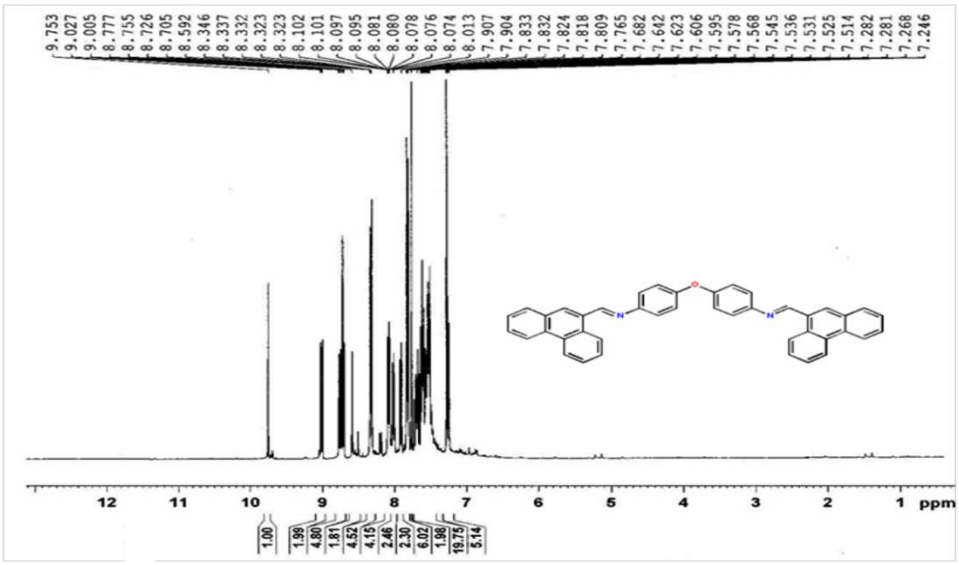

(a)

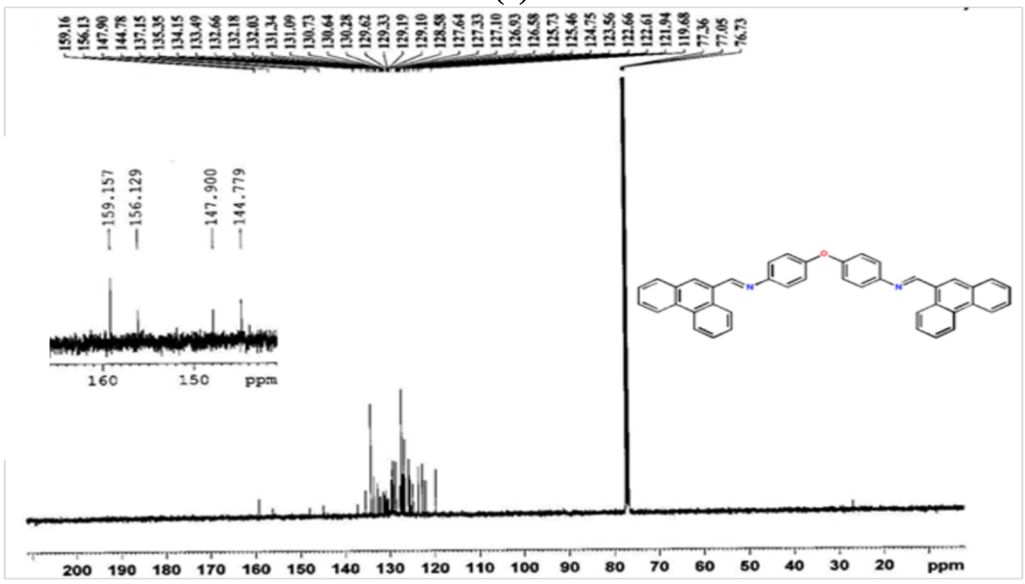

(b)

Annexure 6. NMR spectra for compound **6**; (a) ^{1}H NMR spectrum, (b) ^{13}C NMR spectrum.

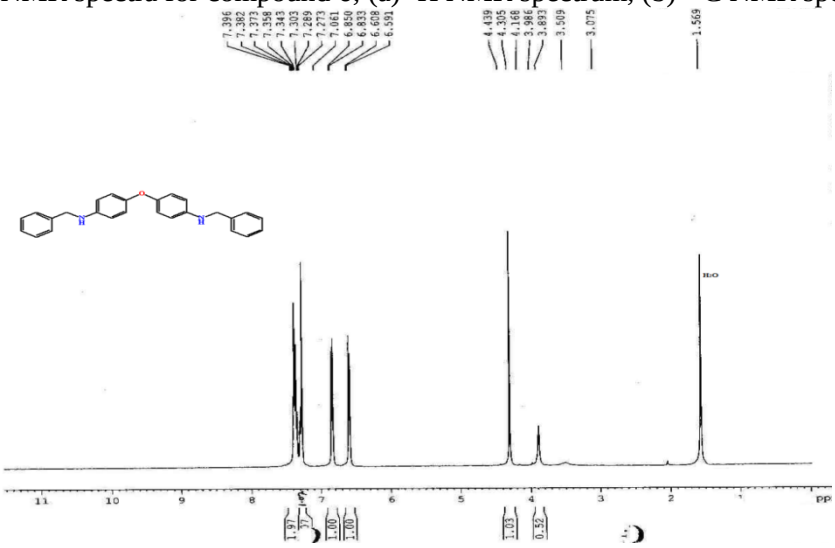

(a)

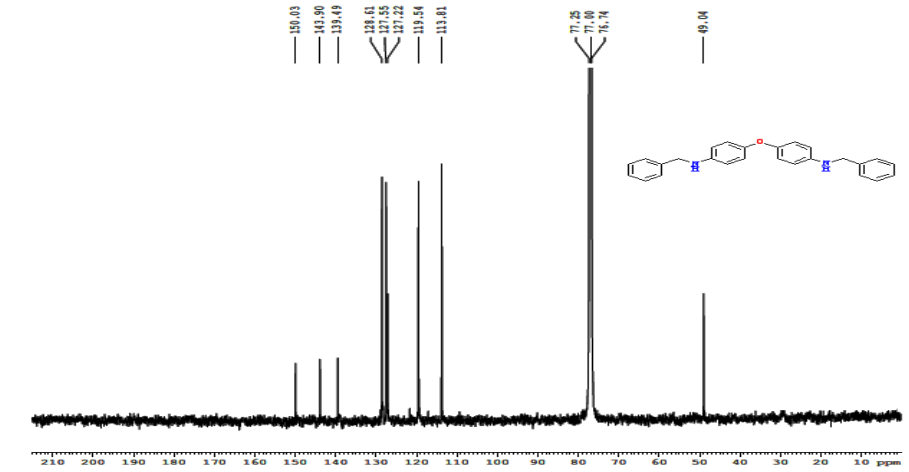

(b)

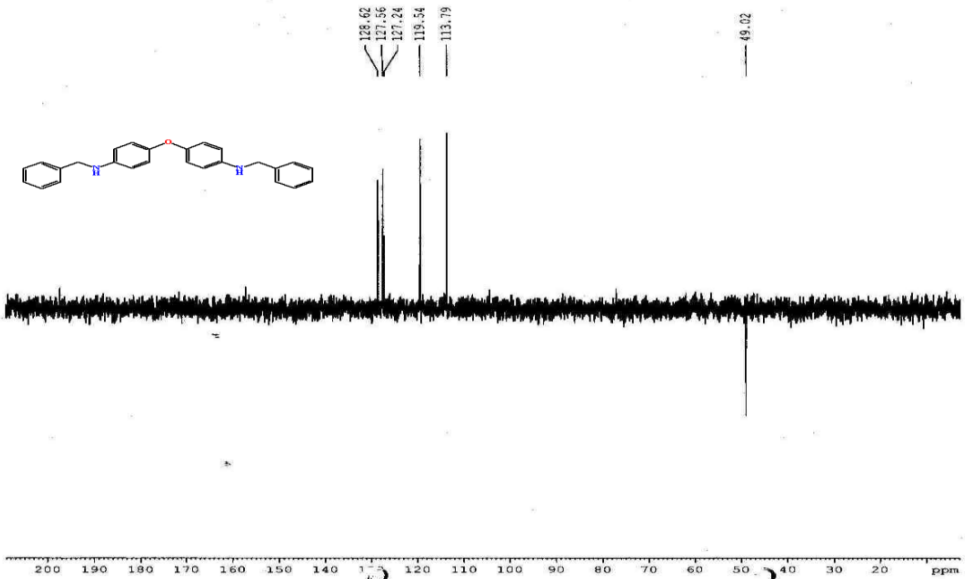

(c)

Annexure 7. NMR spectra for compound **7**; (a) ^{1}H NMR spectrum, (b) ^{13}C NMR spectrum, (c) DEPT-135 NMR spectrum.

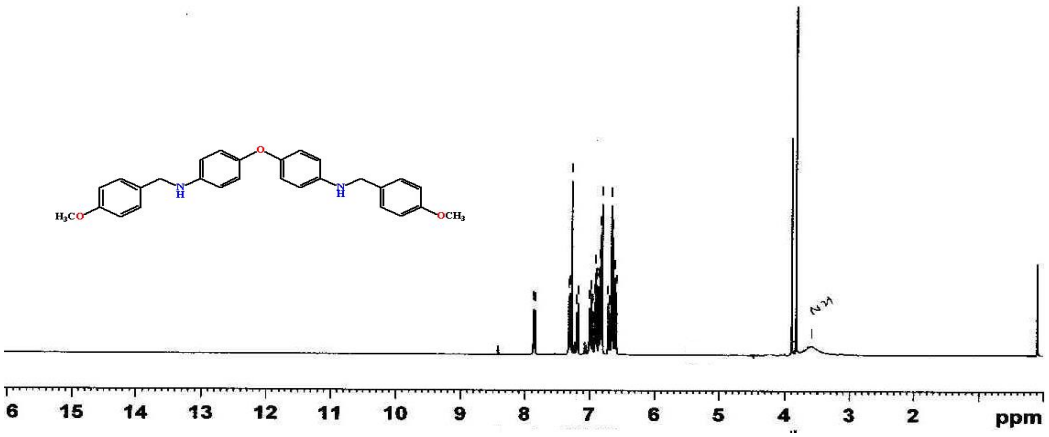

(a)

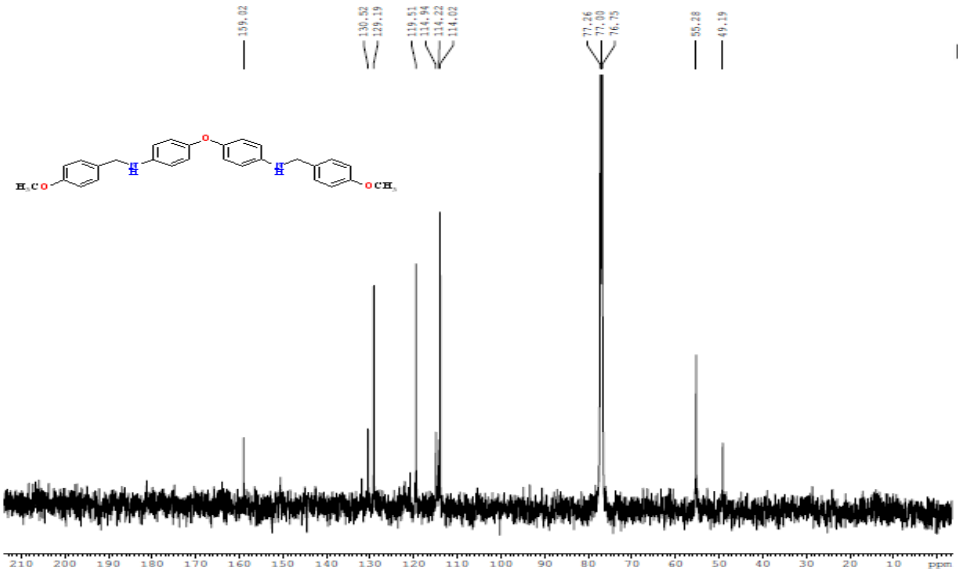

(b)

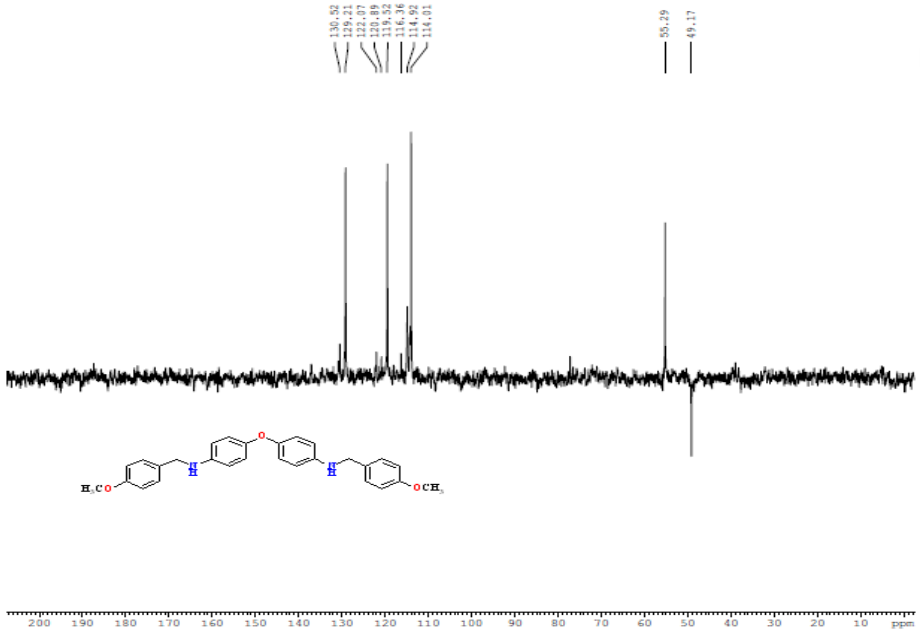

(c)

Annexure 8. NMR spectra for compound **8**; (a) ^{1}H NMR spectrum, (b) ^{13}C NMR spectrum, (c) DEPT-135 NMR spectrum.

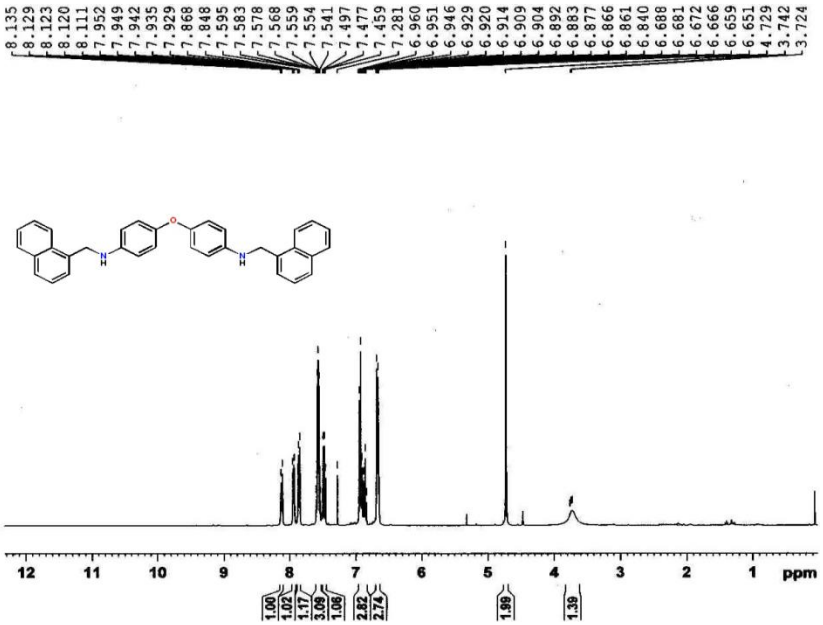

(a)

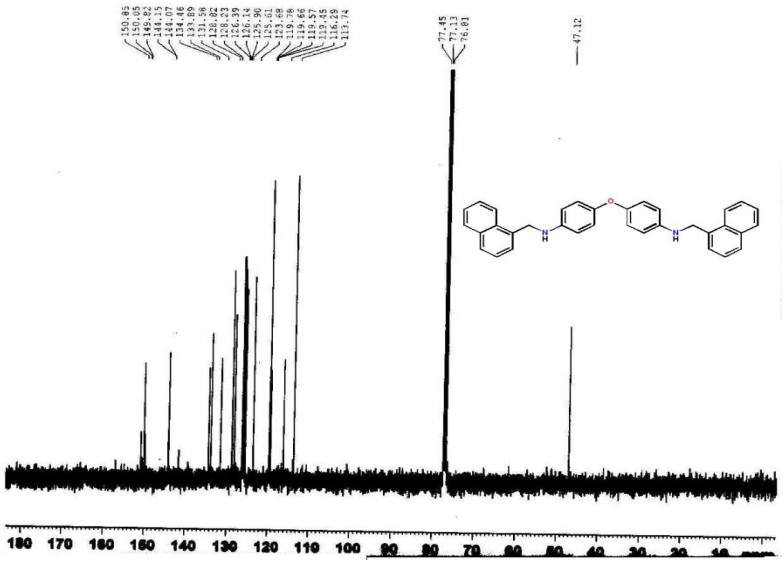

(b)

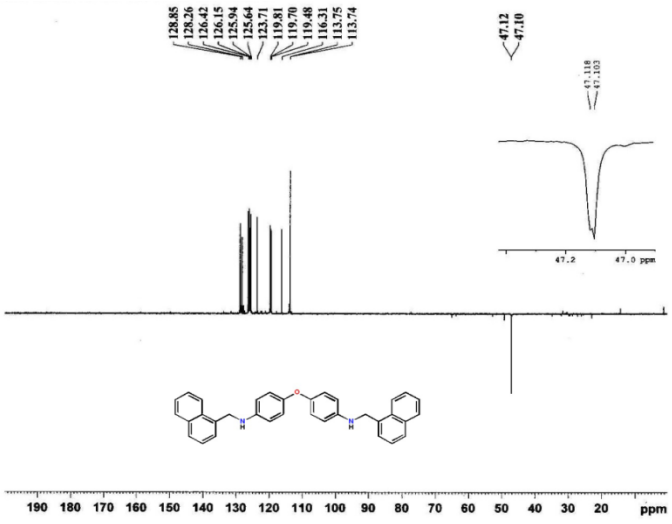

(c)

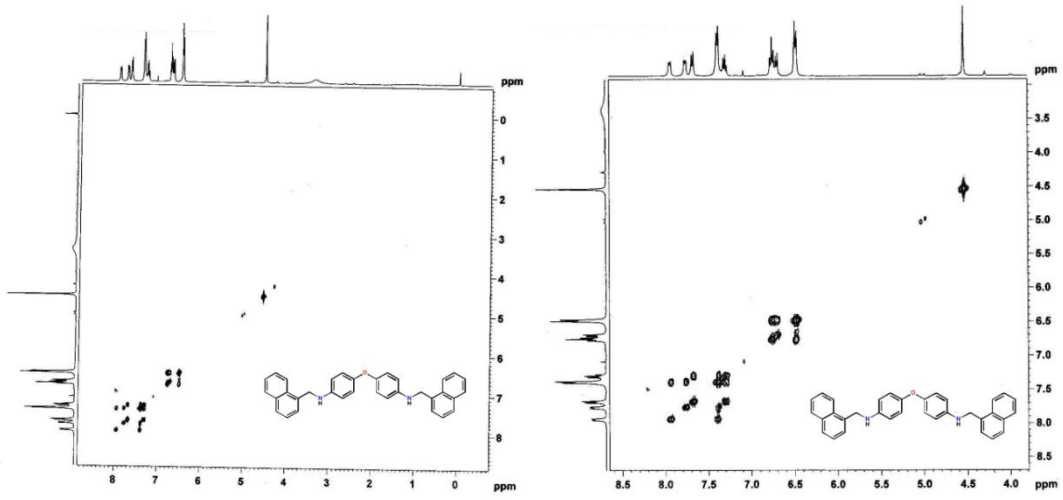

(d)

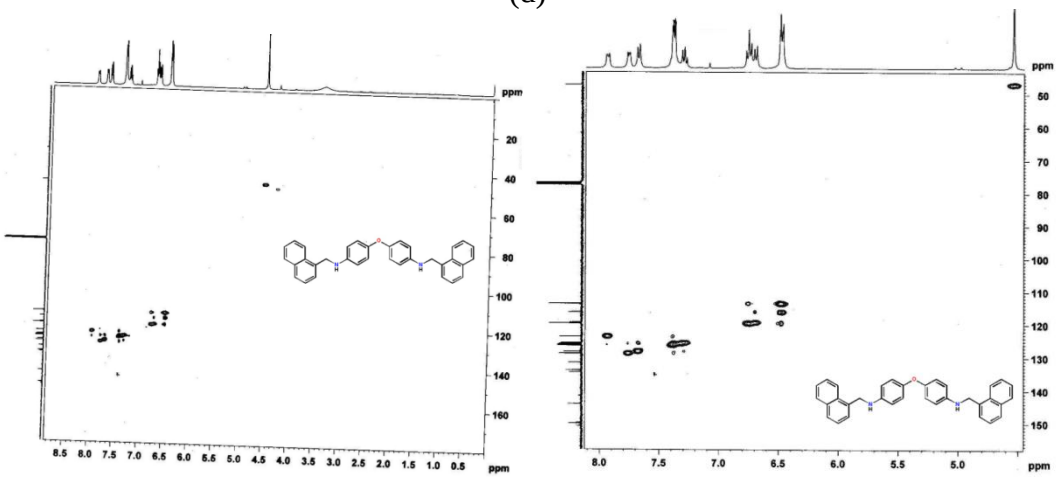

(e)

Annexure 9. NMR spectra for compound **9**; (a) ^{1}H NMR spectrum, (b) ^{13}C NMR spectrum, (c) DEPT-135 NMR spectrum, (d) g-COSY NMR Spectrum, (e) HSQC NMR spectrum.

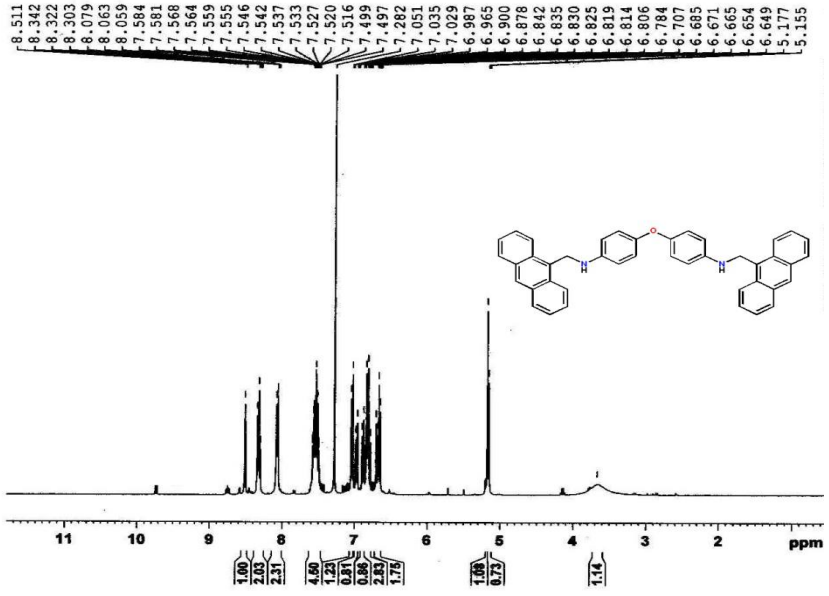

(a)

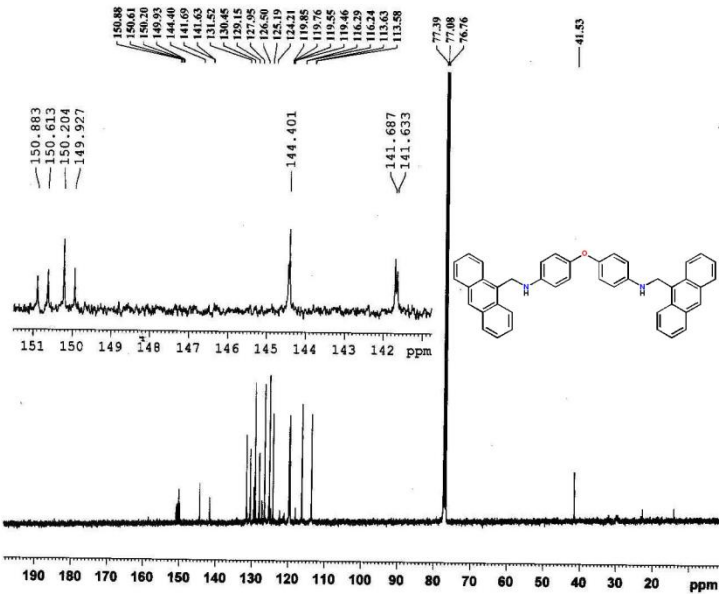
150.883
150.613
150.204
149.927
144.401
141.687
141.633
77.39
77.08
76.76
41.53
151 150 149 148 147 146 145 144 143 142 ppm
190 180 170 160 150 140 130 120 110 100 90 80 70 60 50 40 30 20 ppm

(b)

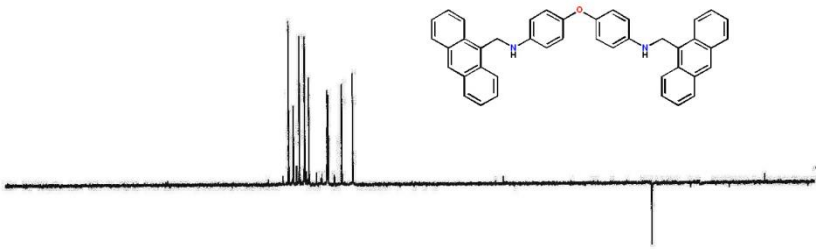

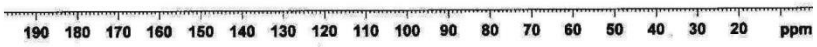
190 180 170 160 150 140 130 120 110 100 90 80 70 60 50 40 30 20 ppm

(c)

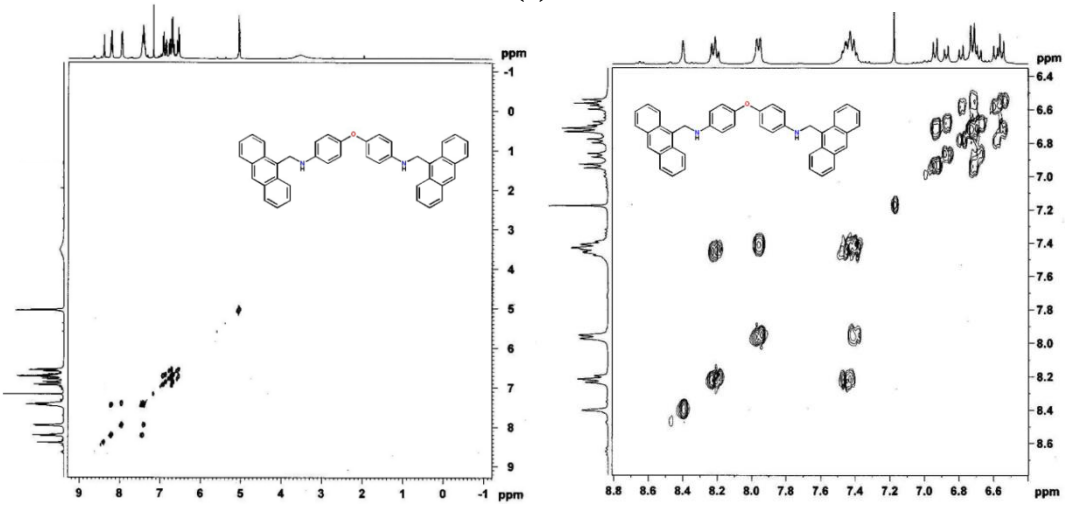
ppm
9 8 7 6 5 4 3 2 1 0 -1 ppm
8.8 8.6 8.4 8.2 8.0 7.8 7.6 7.4 7.2 7.0 6.8 6.6 ppm

(d)

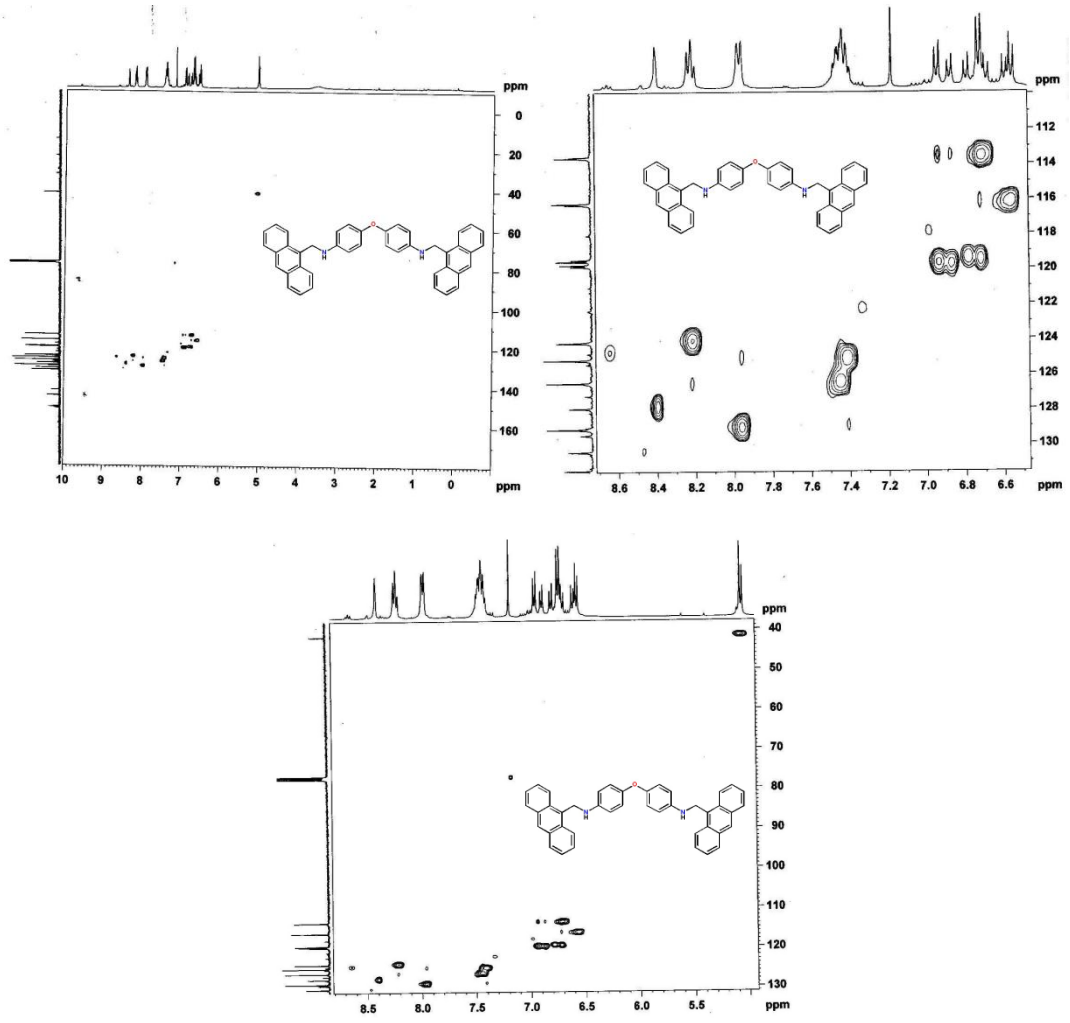

(e)

Annexure 10. NMR spectra for compound **10**; (a) ^{1}H NMR spectrum, (b) ^{13}C NMR spectrum, (c) DEPT-135 NMR spectrum, (d) g-COSY NMR Spectrum, (e) HSQC NMR spectrum.

5A.6.2 *In vitro* cytotoxicity

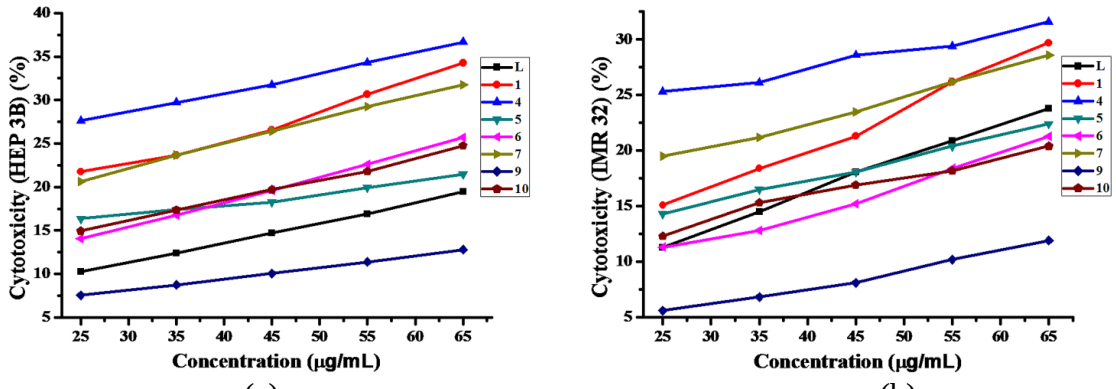

(a) (b)

Annexure 11. Concentration versus % inhibition against (a) HEP 3B cells, (b) IMR 32 cells.